INTERNATIONAL JOURNAL FOR NUMERICAL METHODS IN FLUIDS, VOL. 8, 813–843 (1988)

A FREQUENCY–TIME DOMAIN FINITE ELEMENT MODEL FOR TIDAL CIRCULATION BASED ON THE LEAST-SQUARES HARMONIC ANALYSIS METHOD

J. J. WESTERINK

Ocean Engineering Program, Civil Engineering Department, Texas A & M University, College Station, TX 77843, U.S.A.

J. J. CONNOR AND K. D. STOLZENBACH

Department of Civil Engineering, Massachusetts Institute of Technology, Cambridge, MA 02139, U.S.A.

SUMMARY

An iterative type harmonic finite element model is developed for solving the full non-linear form of the shallow water equations. The scheme iteratively updates time histories of the non-linear terms which are then harmonically decomposed and used as forcing terms for the linear sets of equations which result from the harmonic separation of the shallow water equations.

A least-squares harmonic analysis procedure is used to decompose the non-linear forcing terms. This procedure allows for the very efficient separation of extremely closely spaced harmonics, since it is highly selective with respect to the frequencies it considers. In addition tailoring the procedure and using very specific time steps and sampling periods significantly reduces the number of time samplings points required. In conjunction with the iterative nature of our scheme, the least-squares procedure makes the scheme entirely general, allows for the direct assessment of all tidal constituents, including compound tides, and permits the clear cut and complete investigation of their mutual interaction through the non-linearities. In addition this procedure readily computes very-low-frequency or residual type circulations.

The FE formulation used shows a very low degree of spurious oscillations while remaining quite simple to implement. This control on nodal oscillations is especially important due to the energy transfer mechanisms involved in this type of iterative scheme.

In an example application the effects of the various non-linear overtide and compound tide type interactions are examined. It is demonstrated that not only are compound tides significant relative to the overtides, but they also influence the overtides.

KEY WORDS Shallow Water Equations Iterative Harmonic Analysis Least Squares Finite Element Tides

INTRODUCTION

It is well known that the periodic character of tides stems from the highly periodic nature of the motion of the celestial bodies whose gravitational forces generate them. In fact tides in the deep ocean are described with harmonic constituents whose frequencies are directly associated with the motions of the moon and sun relative to the Earth's surface. Tidal motion is therefore represented by the simple linear superpositioning of the harmonic waves associated with these so called astronomical constituents. As the tides progress into shallower seas and coastal regions, the non-linear terms in the governing equations become significant and the astronomical constituents interact through these non-linearities to generate what are referred to as the shallow water tides.

0271–2091/88/070813–31$15.50

Received 27 August 1986
Revised 21 September 1987

The frequencies of these shallow water constituents appear as integer combinations of the various astronomical frequencies and are classified as either overtides, which correspond to the generation of a response through the non-linearities by one astronomical component, or compound tides, which are the result of the non-linear interaction between two or more astronomical constituents. Only a limited number of shallow water tides are of importance, since their amplitudes generally decrease significantly as energy spreads to higher-order harmonics. Thus owing to the highly periodic nature of the tidal phenomenon, harmonic procedures present themselves as an intrinsically natural framework within which tides can be studied. In fact analytical harmonic or frequency domain solutions have been used in tidal forecasting for more than a century.[1]

Harmonic methods eliminate the time dependence from the governing shallow water equations and produce sets of quasi-steady equations for each of the frequencies present in the tidal spectrum at the site of interest. In deep water these sets of equations are uncoupled and independent, whereas in shallow water they are coupled and interdependent owing to the non-linearities. Hence the application of harmonic methods in shallow waters requires the linearization of the governing equations such that the coupling between the various component equations is retained. This is an especially difficult task when considering the important bottom friction terms.

Upon the advent of the computer era, harmonic methods were abandoned in favour of schemes which discretize the governing shallow water equations in space and time using finite difference (FD) and later finite element (FE) methods. These methods are quite straightforward to apply and make it possible to perform computations in arbitrarily shaped embayments.

Revived interest in the harmonic approach has recently come about due to the inherent advantages offered by working in the frequency domain when periodic phenomena are being considered. To this end a number of modellers[2-5] have been using harmonic methods as an alternative to time-stepping methods while retaining the flexibility offered by a FD or FE discretization in space. Thus the concept of time marching and the problems associated with it are entirely eliminated. However, many of the possibilities offered by this hybrid approach have as yet not been fully exploited. The approach allows for the accurate resolution of daily tidal fluctuations. In addition it readily accounts for beating effects such as spring tide/neap tide variations by simple linear superpositioning of closely spaced astronomical components. Furthermore, both overtide and compound tide constituents can be computed. Finally, concise and direct assessments of long-period or residual fluctuations (steady-state, monthly, etc.) in a tidal embayment are possible from first principles. Each of the above capabilities has the potential of being performed with substantial computational savings over standard time-stepping schemes. These savings can be particularly significant when long-period tidal fluctuations are under consideration.

Harmonic methods necessitate that the non-linearities in the governing equations be dealt with as linear terms while the associated harmonic coupling between the various constituents is accounted for. Strategies to handle this quasi-linearization have consisted of either perturbation analyses[2,6] or some type of iterative procedure which treats non-linearities as right-hand-side forcings which are updated with every cycle.[3,5,7] However, early investigators did not take into account the generation of compound tides, even though they can constitute a significant part of the shallow water constituent spectrum and can indeed play an important role in the correct distribution of the entire spectrum. More recently Le Provost[8,9] has developed a harmonic-based FE model which does take into account compound tides. He applies a perturbation analysis and a quasi-linearization for bottom friction such that the non-linear coupling between the various astronomical constituents can be accounted for.

In the development of our harmonic-based tidal circulation model, we have selected an iterative approach in conjunction with a harmonic analysis technique based on the rigorous application of the least-squares method. The least-squares harmonic analysis method is able to extract extremely closely and irregularly spaced frequency information in a very efficient manner.[1,10,11] This entirely general procedure allows for the direct assessment of all the tidal constituents, including the compound tides, and permits the clear cut and complete investigation of their mutual interaction through the non-linearities. Furthermore, we have included the study of the low-frequency end of the shallow water constituent spectrum. The capability of evaluating long-period fluctuations, which may be regarded as comprising the Eulerian residual circulation, is an especially salient feature which naturally results from our procedure without necessarily increasing the computational effort. Finally we have selected the Galerkin FE method to resolve the spatial dependence in the governing shallow water equations. We have taken care to formulate our numerical solution procedure such that it neither promotes significant spurious oscillations nor overdamps the fundamental solution, problems which have plagued numerical modellers in the past. Indeed it is vital to the success of our iterative solution procedure to limit the extent of spurious oscillations. This is because of the nature of the cascading forcing mechanisms which drive the shallow water constituents in our iterative harmonic solution and the associated forcing signal-to-noise ratios which could prematurely undermine the integrity of the computed higher-order harmonics if severe spurious oscillations were present. In subsequent sections we shall describe the details of the harmonic-based FE model TEA-NL (non-linear tidal embayment analysis) and illustrate the various non-linear interactions that are caused by the finite amplitude and non-linear friction terms for both an overtide and compound tide situation.

GOVERNING EQUATIONS

The equations used to describe tidal wave propagation are the shallow water equations which are derived by integrating the conservation of momentum and continuity equations over depth and are expressed as

$$u_{,t}+g\eta_{,x}-fv+c_f\frac{(u^2+v^2)^{1/2}}{h+\eta}u+(uu_{,x}+vu_{,y})=0, \tag{1a}$$

$$v_{,t}+g\eta_{,y}+fu+c_f\frac{(u^2+v^2)^{1/2}}{h+\eta}v+(uv_{,x}+vv_{,y})=0, \tag{1b}$$

$$\eta_{,t}+[u(h+\eta)]_{,x}+[v(h+\eta)]_{,y}=0, \tag{2}$$

where

t	time
x, y	Cartesian co-ordinates
u, v	depth-averaged components of velocity in the x, y co-ordinate directions
η	surface elevation relative to mean sea level (MSL)
h	depth to MSL
g	acceleration due to gravity
f	Coriolis factor
c_f	bottom friction coefficient.

The non-linearities which cause the coupling between harmonic constituents and are responsible for the generation of the shallow water tides consist of bottom friction and convective acceler-

ation terms in the momentum equations and finite amplitude effects in both the momentum (where they appear in the bottom friction term) and continuity equations.

The boundary conditions associated with the governing equations are the prescription of elevation, η^*, and the prescription of normal flux, Q_n^*, which are respectively expressed as

$$\eta(x, y, t) = \eta^*(x, y, t) \qquad \text{on } \Gamma_\eta, \tag{3a}$$

$$Q_n(x, y, t) = Q_n^*(x, y, t) \qquad \text{on } \Gamma_Q. \tag{3b}$$

Elevation-prescribed boundaries usually coincide with the open ocean boundary, while the normal-flux-prescribed boundary typically represents land and river boundaries. It is noted that normal flux may be expressed as

$$Q_n = \alpha_{nx}[u(h+\eta)] + \alpha_{ny}[v(h+\eta)], \tag{4}$$

where α_{nx} and α_{ny} are the direction cosines on the boundary.

DEVELOPMENT OF THE DISCRETE HARMONIC FORM OF THE GOVERNING EQUATIONS

Our formulation works with the unmodified or so called primitive form of the shallow water equations. The scheme used, referred to as the primitive pseudo-wave equation (PPWE) formulation, shows very well controlled behaviour with respect to nodal oscillations while keeping the number of terms to a strict minimum. A detailed description and analysis of the PPWE formulation is given by Westerink *et al.*[12].

Weighted residual formulation

The PPWE scheme is based on establishing a weak weighted residual form of the continuity equation and thus treating elevation-prescribed boundary conditions as essential and normal-flux-prescribed boundary conditions as natural. Applying Galerkin's method, the error in the continuity equation is weighted by the variation in elevation, $\delta\eta$, and is integrated over the interior domain Ω. Furthermore, the natural boundary error is accounted for by weighting the error in the normal boundary flux with $\delta\eta$ and integrating over the flux-prescribed boundary Γ_Q. It is required that these combined errors vanish and the following expression results:

$$\int\int_\Omega \{\eta_{,t} + [u(h+\eta)]_{,x} + [v(h+\eta)]_{,y}\}\delta\eta \, d\Omega + \int_{\Gamma_Q} (-Q_n + Q_n^*)\delta\eta \, d\Gamma = 0. \tag{5}$$

Applying Gauss's theorem and taking into account relationship (4) and the fact that $\delta\eta$ vanishes on the essential boundary leads to the symmetrical weak weighted residual form. Moving the non-linear and boundary loading terms to the right-hand side yields

$$\int\int_\Omega [\eta_{,t}\delta\eta - uh(\delta\eta)_{,x} - vh(\delta\eta)_{,y}] \, d\Omega = -\int_{\Gamma_Q} Q_n^*\delta\eta \, d\Gamma + \int\int_\Omega [u\eta(\delta\eta)_{,x} + v\eta(\delta\eta)_{,y}] \, d\Omega. \tag{6}$$

The weighted residual forms of the momentum equations are obtained by weighting the associated errors with the residual velocities and integrating over the interior domain. Again the non-linearities are taken to the right-hand side. Furthermore, in order to enhance iterative stability, a linearized friction term is included on both sides of each equation. Finally, both equations are multiplied through by depth to allow for symmetry in the derivative matrices which will appear in both the discretized continuity and momentum equations. With these modifi-

cations the weighted residual forms of the momentum equations appear as

$$\iint_\Omega (hu_{,t} + gh\eta_{,x} - fhv + \lambda u)\delta u \, d\Omega = \iint_\Omega \left(\lambda u - c_f \frac{h}{h+\eta}(u^2+v^2)^{1/2}u - h(uu_{,x} + vu_{,y})\right)\delta u \, d\Omega, \tag{7}$$

$$\iint_\Omega (hv_{,t} + gh\eta_{,y} + fhu + \lambda v)\delta v \, d\Omega = \iint_\Omega \left(\lambda v - c_f \frac{h}{h+\eta}(u^2+v^2)^{1/2}v - h(uv_{,x} + vv_{,y})\right)\delta v \, d\Omega. \tag{8}$$

Equations (6)–(8) serve as the basis of the FE formulation. All non-linear terms appear on the right-hand sides, where they can be conveniently updated with each iteration as non-linear force loadings to a linear problem.

Application of the finite element method

In order to generate a system of algebraic equations from integral equations, the FE method is applied to the final form of the weighted residual equations. To satisfy the minimum functional continuity requirements on the variables, interpolating bases with at least C^0 functional continuity must be used for the FE approximations. Identical type and order bases are used for the dependent variables, elevation and velocities. In addition the same elemental approximations are used for prescribed normal flux, mean water level depths, bottom friction coefficient and linearized friction factor as are used for the dependent variables. In this manner the dependent variables and the parameters will all be defined at the same set of nodes. Thus the variables and parameters may be expressed within each element in the following form:

$$a(x, y, t) = \boldsymbol{\phi}(x, y)\mathbf{a}^{(n)}(t) \tag{9}$$

where

$a(x, y, t)$	representative variable which stands for u, v, η, h, λ, c_f and the variations δu, δv and $\delta\eta$
$\boldsymbol{\phi}(x, y)$	elemental vector of C^0 interpolating polynomials
$\mathbf{a}^{(n)}(t)$	elemental vector of nodal values for the representative variable.

Substituting the elemental expansions of the form (9) into (6)–(8), summing over all the elements within the domain and accounting for the arbitrary variation of δu, δv and $\delta\eta$ leads to a set of non-linear algebraic equations which constrain the weighted error incurred in the continuity and momentum equations due to the finite spatial representation of the variables. These global FE equations for continuity and momentum are respectively expressed as

$$\mathbf{M}_\eta \boldsymbol{\eta}_{,t} - \mathbf{D}\mathbf{U} = \mathbf{P}_\eta^{\text{lin}} + \mathbf{P}_\eta^{\text{nl}}, \tag{10}$$

$$\mathbf{M}_U \mathbf{U}_{,t} + \mathbf{M}_F\mathbf{U} + \mathbf{M}_C\mathbf{U} + g\mathbf{D}^T\boldsymbol{\eta} = \mathbf{P}_{\Delta-\text{fric}}^{\text{nl}} - \mathbf{P}_{\text{conv}}^{\text{nl}}, \tag{11}$$

where

$\boldsymbol{\eta}$	global elevation vector
$\mathbf{U}$	global velocity vector
$\mathbf{M}_\eta$	global continuity equation coefficient matrix
$\mathbf{M}_U$	global momentum equation mass matrix
$\mathbf{M}_F$	global linearized friction distribution matrix
$\mathbf{M}_C$	global Coriolis matrix
$\mathbf{P}_\eta^{\text{lin}}$	global load vector for flux-prescribed boundaries
$\mathbf{P}_\eta^{\text{nl}}$	global load vector for continuity equation finite amplitude effects

$\mathbf{P}^{\mathrm{nl}}_{\Delta-\mathrm{fric}}$ global load vector containing the difference between linearized friction and full non-linear friction terms

$\mathbf{P}^{\mathrm{nl}}_{\mathrm{conv}}$ global load vector representing convective acceleration effects.

Each of these global matrices and vectors is assembled using the appropriate elemental sub-matrices and vectors. In particular the various global load vectors are computed using the following elemental vectors:

$$\mathbf{P}^{(n),\,\mathrm{lin}}_{\eta} = \left[\int_{\Gamma_Q} \boldsymbol{\phi}^{\mathrm{T}} Q^*_{\mathrm{n}} \, \mathrm{d}\Gamma \right], \tag{12}$$

$$\mathbf{P}^{(n),\,\mathrm{nl}}_{\eta} = \left[\int\int_{\Omega_e} (\boldsymbol{\phi}^{\mathrm{T}}_{,x} \eta u + \boldsymbol{\phi}^{\mathrm{T}}_{,y} \eta v) \, \mathrm{d}\Omega \right], \tag{13}$$

$$\mathbf{P}^{(n),\,\mathrm{nl}}_{\Delta-\mathrm{fric}} = \begin{bmatrix} \displaystyle\int\int_{\Omega_e} \boldsymbol{\phi}^{\mathrm{T}} \left(\lambda u - c_{\mathrm{f}} \frac{h}{h+\eta} (u^2+v^2)^{1/2} u \right) \mathrm{d}\Omega \\ \displaystyle\int\int_{\Omega_e} \boldsymbol{\phi}^{\mathrm{T}} \left(\lambda v - c_{\mathrm{f}} \frac{h}{h+\eta} (u^2+v^2)^{1/2} v \right) \mathrm{d}\Omega \end{bmatrix}, \tag{14}$$

$$\mathbf{P}^{(n),\,\mathrm{nl}}_{\mathrm{conv}} = \begin{bmatrix} \displaystyle\int\int_{\Omega_e} \boldsymbol{\phi}^{\mathrm{T}} h (u u_{,x} + v u_{,y}) \mathrm{d}\Omega \\ \displaystyle\int\int_{\Omega_e} \boldsymbol{\phi}^{\mathrm{T}} h (u v_{,x} + v v_{,y}) \mathrm{d}\Omega \end{bmatrix} \tag{15}$$

For the development of our computer code, TEA-NL, it was felt that the simplicity of linear C^0 bases outweighed the improved accuracy achieved (for the same number of nodes) with higher-order elements. Therefore the simplest possible element, the linear triangle, was selected to represent the variation of the variables and parameters within each element.

Spectral decomposition of the governing equations

The FE technique has eliminated the differential spatial dependence from the shallow water equations. However, the resulting systems of equations (10) and (11) remain differentially time-dependent. This time dependence is resolved by reducing (10) and (11) to sets of harmonic equations which are coupled through the non-linear terms.

The variables $\boldsymbol{\eta}$ and $\mathbf{U}$ and the loadings $\mathbf{P}^{\mathrm{lin}}_{\eta}$, $\mathbf{P}^{\mathrm{nl}}_{\eta}$, $\mathbf{P}^{\mathrm{nl}}_{\Delta-\mathrm{fric}}$ and $\mathbf{P}^{\mathrm{nl}}_{\mathrm{conv}}$ are all time-dependent vectors. It is assumed that these responses and both linear and non-linear load vectors may be expressed as harmonic series of the form

$$\mathbf{A}(t) = \mathrm{Re}\left(\sum_{j=1}^{N_{\mathrm{f}}} \hat{\mathbf{A}}_j \mathrm{e}^{\mathrm{i}\omega_j t} \right), \tag{16}$$

where

$\mathbf{A}(t)$ representative vector which stands for the time history of the responses $\boldsymbol{\eta}$ and $\mathbf{U}$ and any of the load vectors

$\hat{\mathbf{A}}_j$ complex amplitudes of the jth harmonic constituent of $\mathbf{A}(t)$; both magnitude and phase shift are represented

i $(-1)^{1/2}$

ω_j jth frequency of the spectrum

N_f number of frequencies required to adequately represent the significant constituents of the tidal spectrum.

Substituting the harmonic series representation for each of the responses and load vectors into (10) and (11) leads to N_f sets of time-independent linear systems of equations of the following form:

$$i\omega_j \mathbf{M}_\eta \hat{\boldsymbol{\eta}}_j - \mathbf{D}\hat{\mathbf{U}}_j = \hat{\mathbf{P}}^{\text{lin}}_{\eta_j} + \hat{\mathbf{P}}^{\text{nl}}_{\eta_j}, \tag{17}$$

$$i\omega_j \mathbf{M}_U \hat{\mathbf{U}}_j + \mathbf{M}_F \hat{\mathbf{U}}_j + \mathbf{M}_C \hat{\mathbf{U}}_j + g\mathbf{D}^T \hat{\boldsymbol{\eta}}_j = \hat{\mathbf{P}}^{\text{nl}}_{\Delta-\text{fric}_j} - \hat{\mathbf{P}}^{\text{nl}}_{\text{conv}_j}. \tag{18}$$

It is noted that the natural-flux-prescribed boundary conditions are included in the load vectors $\hat{\mathbf{P}}^{\text{lin}}_{\eta_j}$. The essential boundary conditions may also be expressed as a harmonic series of the form (16), which leads to a set of essential boundary conditions associated with each set of equations (17) and (18) of the form

$$\hat{\eta}_j|_{\Gamma_\eta} = \hat{\eta}^*_j. \tag{19}$$

All sets of equations (17) and (18) are in themselves linear and independent for every frequency ω_j at each specific cycle of the iterative solution procedure. However, the non-linearities do couple the various sets of equations between iterative cycles when the non-linear load vectors are re-evaluated using the sum of all the updated non-zero responses at the frequencies present in the spectrum. The non-linear load vectors are computed as time histories which are then harmonically decomposed and distributed to various frequencies.

SOLUTION TO THE LINEAR EQUATIONS

The harmonic decoupling of the governing equations with the explicit linearization through the iterative scheme led to a set of time-independent linear equations (17) and (18) of the same genera form for each frequency in the spectrum. These equations form the core of our fully non-linear scheme and must be solved for all the frequencies of importance in the tidal spectrum at each cycle of the iteration until convergence is reached. Therefore it is important that the linear core solution strategy be not only accurate and free of spurious oscillations but also very efficient.

The PPWE formulation solves each of these linear sets of equations (17) and (18) by forming a pseudo-wave equation with $\hat{\boldsymbol{\eta}}$ as the basic variable by substituting the discretized momentum equation (18) into the discretized continuity equation (17). Thus the momentum equation (18) is solved for $\hat{\mathbf{U}}_j$ as follows:

$$\hat{\mathbf{U}}_j = \hat{\mathbf{M}}^{-1}_{\text{TOT}}(\hat{\mathbf{P}}^{\text{nl}}_{\Delta-\text{fric}_j} - \hat{\mathbf{P}}^{\text{nl}}_{\text{conv}_j} - g\mathbf{D}^T \hat{\boldsymbol{\eta}}_j) \tag{20}$$

where

$$\hat{\mathbf{M}}_{\text{TOT}} = (i\omega_j \mathbf{M}_U + \mathbf{M}_F + \mathbf{M}_C). \tag{21}$$

Substituting for $\hat{\mathbf{U}}_j$ into the discretized continuity equation produces

$$(i\omega_j \mathbf{M}_\eta + g\mathbf{D}\hat{\mathbf{M}}^{-1}_{\text{TOT}}\mathbf{D}^T)\hat{\boldsymbol{\eta}}_j = -\hat{\mathbf{P}}^{\text{lin}}_{\eta_j} + \hat{\mathbf{P}}^{\text{nl}}_{\eta_j} + \mathbf{D}\hat{\mathbf{M}}^{-1}_{\text{TOT}}(\hat{\mathbf{P}}^{\text{nl}}_{\Delta-\text{fric}_j} - \hat{\mathbf{P}}^{\text{nl}}_{\text{conv}_j}). \tag{22}$$

The final system matrix of (22) is complex, non-symmetric (since the Coriolis matrix $\mathbf{M}_C$ is contained in $\hat{\mathbf{M}}_{\text{TOT}}$) and has frequency embedded into it. Because of core storage limitations it is preferable to reset and resolve the system matrix for each frequency at each cycle of the iteration rather than storing the matrix produced for each frequency at the first cycle and using it in

subsequent cycles. After solving for $\hat{\boldsymbol{\eta}}_j$ with (22), we substitute for $\hat{\boldsymbol{\eta}}_j$ into (20) and solve directly for $\hat{\mathbf{U}}_j$.

It is noted that schemes which attempt to generate frequency-independent, symmetrical and real matrices require iterative type solution procedures for each linear system of equations (owing to linear variable terms having to be moved to the right-hand side to accomplish the desired system matrix properties). This iteration for each linear solution is distinct from the iteration scheme discussed in the previous section which updated the non-linear terms in the governing equations. Schemes which produce system matrices which do not involve frequency ω_j are desirable in that they eliminate the need to reset and resolve a different system matrix for each of the many frequencies required for the fully non-linear solution. However, these procedures proved to be impractical for use as linear core solvers due to potential convergence rate and/or iterative stability problems.

The PPWE scheme solves for elevation and velocity sequentially through the formation of the pseudo-wave equation. This equation rearrangement provides the potential for significant reductions in computational effort when compared with schemes which solve for elevation and velocity simultaneously. In order to ensure this improved computational efficiency, the mass matrix $\mathbf{M}_U$, the linearized frictional distribution matrix $\mathbf{M}_F$ and the Coriolis matrix $\mathbf{M}_C$ must all be lumped such that the inversion of $\mathbf{M}_{TOT}$ in equations (20) and (22) does not lead to a fully populated matrix. Lumping is not required for the continuity equation coefficient matrix $\mathbf{M}_\eta$. In fact $\mathbf{M}_\eta$ is not lumped in order to improve the phase properties of the PPWE scheme. The lumping procedures in effect amount to a spatial redistribution of mass and the linear friction and Coriolis forcings onto the nodes. They ensure that the system matrix of (22) remains banded and allows for the extremely economical solution of $\hat{\mathbf{U}}_j$ as a result of the tridiagonal partitional structure of $\hat{\mathbf{M}}_{TOT}$. Thus the PPWE scheme allows for the efficient linear solution for each of the frequencies of importance owing to the fact that the solutions for elevation and velocity have been decoupled and owing to the structure of the matrices which result when partial lumping is used.

Westerink *et al.*[12] apply the PPWE scheme to a set of two-dimensional test problems with a geometry consisting of a quarter of an annulus and including a number of different depth variations. These applications show that the PPWE scheme leads to excellent solutions exhibiting a very low degree of spurious oscillations. This indicates that it is possible to obtain high-quality numerical solutions using equal-order interpolation for both elevation and velocities with a formulation based directly on the primitive shallow water equations. The extent of spurious oscillations is qualitatively similar to that of the semi-implicit method (SIM) formulation of Gray and Lynch,[13] although it is not quite as well controlled as the wave equation (WE) formulation of Lynch and Gray.[14] However, the PPWE scheme is a simpler formulation than either the SIM or WE formulation since it is based directly on the primitive equations. This simplicity is important with regard to the efficiency of the scheme and is especially significant when an iterative non-linear formulation such as ours is under consideration.

The PPWE scheme's control on spurious oscillations is not directly related to the formation of the pseudo-wave equation nor to any similarities with respect to either the SIM or WE schemes. In fact it can be readily shown that for a harmonic formulation the SIM and WE schemes are identical. It is shown by Westerink *et al.*[12] that the PPWE scheme's success stems entirely from the boundary condition treatment for which elevation is taken as an essential boundary condition and the flux boundary condition is relaxed and treated as a natural condition. Handling the boundary conditions in this fashion is suggested by the formation of the pseudo-wave equation which is solved first and has elevation as its basic variable. The success achieved by this novel boundary condition treatment emphasizes the importance of the way in which the boundary conditions are handled for the primitive equations. It is noted that previous investigations of

other alternative boundary condition treatments found that boundary condition treatment was of secondary importance to the actual equation formulation in suppressing numerical oscillations (e.g. Lynch[15]).

SOLUTION TO THE NON-LINEAR EQUATIONS

The non-linear terms in the shallow water equations have been included as right-hand-side harmonic load terms which are updated with information from the previous cycle of our iterative procedure. The iterative solution strategy, presented schematically in Figure 1, starts out with the assumption that these non-linear loadings are zero. The initial forcings to the system will then be entirely linear and consist only of a set of N_b harmonic elevation-prescribed and harmonic normal-flux-prescribed boundary condition components for a set of specified frequencies. The frequencies associated with these non-zero boundary conditions may be associated with both astronomical tidal frequencies and shallow water tidal frequencies depending on the location, depth and geometry of the forcing boundaries. Each of the linear sets of equations (17)–(19) associated with the specified non-zero boundary forcing frequencies are then solved for the given geometry. This then yields harmonic solutions for the variables in the form of amplitudes and phase shifts at the nodes for each frequency. This allows time histories for the responses in elevations and velocities to be generated with (16). Time histories of the non-linear load vectors $\mathbf{P}^{nl}_{\eta}(t)$, $\mathbf{P}^{nl}_{\Delta-fric}(t)$ and $\mathbf{P}^{nl}_{conv}(t)$ can now be produced using the response time histories and (13)–(15).

As was assumed earlier, these time domain non-linear loadings may be represented approximately by a finite harmonic series. The harmonic decomposition of the non-linear forcing vectors produces harmonic loadings at some set of N_h frequencies. We must now examine the relative importance of each of these N_h harmonic non-linear loadings and select only the ones which will significantly influence our solutions. Thus we update the set of N_f frequencies for which the linear model is run by including both boundary and non-linear forcing frequencies of importance. It is noted that significant non-linear forcing frequencies, which were not present in the initial boundary forcing set of frequencies, may appear at either this stage or some later point in the iterative process depending on the non-linearity which generates them. Now each of the N_f linear sets of equations is solved for again. Non-linear effects are explicitly included and therefore the interactions with other frequencies are accounted for. The entire procedure is repeated until convergence is reached.

Harmonic analysis of the non-linear forcing vectors

The selection of a harmonic analysis procedure for the non-linear forcing vectors is of vital importance for the efficiency, accuracy and generality of our non-linear model. Efficiency is determined by the total number of frequencies as well as the total number of time history points required for the harmonic analysis procedure. The accuracy and generality of the harmonic analysis relate to the type and the detail of harmonic information extracted from a given time history record.

A variety of Fourier harmonic analysis procedures can be applied to convert time history loadings to harmonic loadings. Standard Fourier procedures operate with integer multiples of some base frequency. Therefore standard Fourier analysis is quite satisfactory when examining only one major astronomical tide and its overtides. However, as is seen in Table I and depicted graphically in Figure 2, tidal harmonics are not limited to frequencies which are integer multiples of some base frequency. Tidal energy is in general irregularly distributed over a wide range of frequencies. The harmonic components are extremely closely and unevenly grouped within

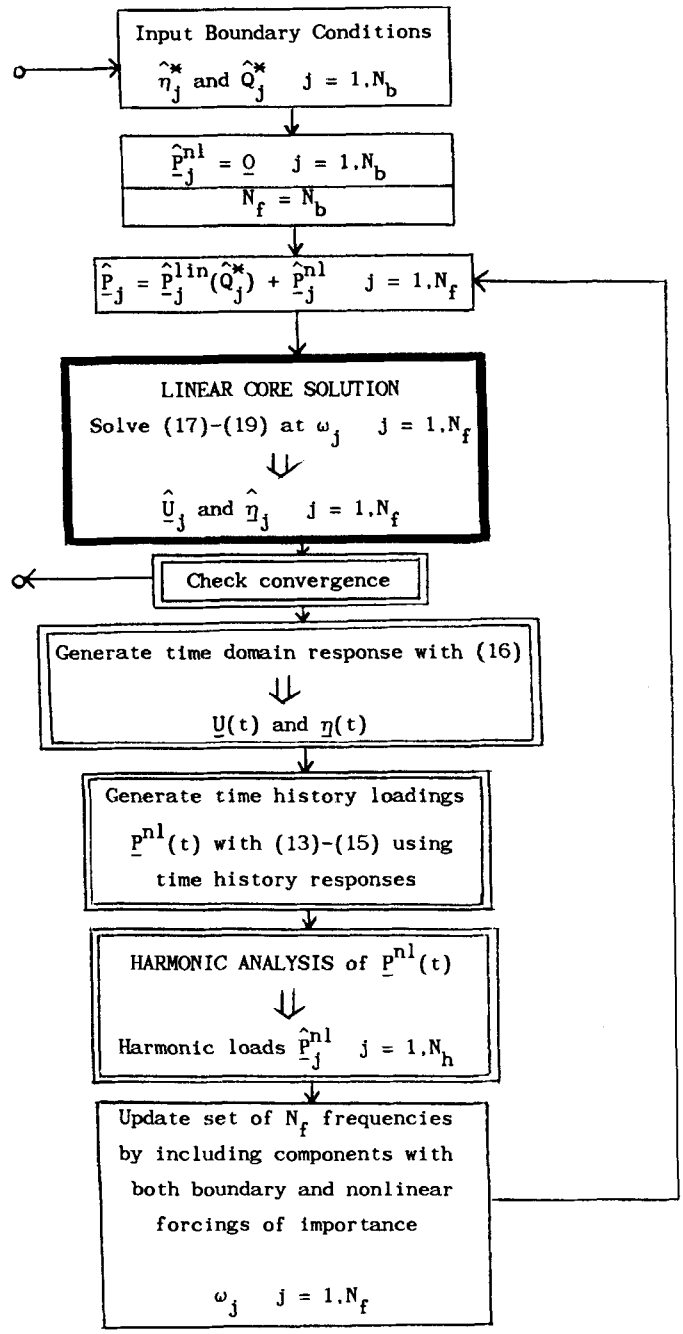

Figure 1. Schematic of iterative non-linear scheme. $\hat{\mathbf{P}}_j^{nl}$ and $\mathbf{P}^{nl}(t)$ generically represent the non-linear load vectors. Solid boxes represent important computations which lend themselves to parallel processing with respect to individual frequency components, whereas double-lined boxes lend themselves to parallel processing on a nodal basis

widely spaced clusters. Hence, in order to obtain sufficient frequency resolution when Fourier analysing the non-linear forcing time histories, an extremely small base frequency step is required. Corresponding to this very small frequency step is a very large total number of frequencies being processed, most of which have no associated tidal energy. With the finer frequency resolution comes a requirement for longer time history records and a larger total number of time sampling points.[16,17] Thus standard Fourier analysis methods would be impractical owing to the excessive amount of numerical effort required to obtain the frequency resolution needed to separate important tidal components.

An extremely attractive alternative to standard Fourier analysis procedures is the least-squares harmonic analysis method.[1,10,11,18] This procedure consists simply of a common least-squares error minimization process which uses a harmonic series as the fitting function. However, the procedure is highly selective with respect to the frequencies it considers and in fact the harmonic series used only contains frequencies which are known to exist in the time history record. Furthermore, the theoretical number of time history sampling points required (for a noise-free signal) is equal to only twice the number of frequencies contained in the time history record. Therefore unlike standard Fourier procedures the number of time history points is entirely

Table I. A list of possibly important astronomical (A), overtide (O) and compound (C) tidal constituents

Tide	Type	Frequency (rad s^{-1})	Period (h)
Steady	O	0·00000000000	—
Ssa	A	0·00000039821	4382·92
MN	C	0·00000263920	661·31
Mm	A	0·00000263920	661.31
SM	C	0·00000492520	354·37
Mf	A	0·00000532341	327·88
O_1	A	0·00006759775	25·82
P_1	A	0·00007252294	24·07
K_1	A	0·00007292117	23·93
$2MK_2$	C	0·00013519550	12·91
$2MS_2$	C	0·00013559371	12·87
N_2	A	0·00013787971	12·66
$3MSN_2$	C	0·00013823292	12·63
M_2	A	0·00014051892	12·42
$2MN_2$	C	0·00014315812	12·19
L_2	A	0·00014315812	12·19
S_2	C	0·00014544412	12·00
K_2	A/O	0·00014584233	11·97
MSN_2	C	0·00014808332	11·79
$2SM_2$	C	0·00015036932	11·61
MN_4	C	0·00027839863	6·27
M_4	O	0·00028103783	6·21
MS_4	C	0·00028596304	6·10
MK_4	C	0·00028636125	6·09
$2MN_6$	C	0·00041891755	4·17
M_6	O	0·00042155675	4·14
MSN_6	C	0·00042384275	4·12
$2MS_6$	C	0·00042648195	4·09
$2MK_6$	C	0·00042688017	4·09
$2SM_6$	C	0·00043140716	4·05

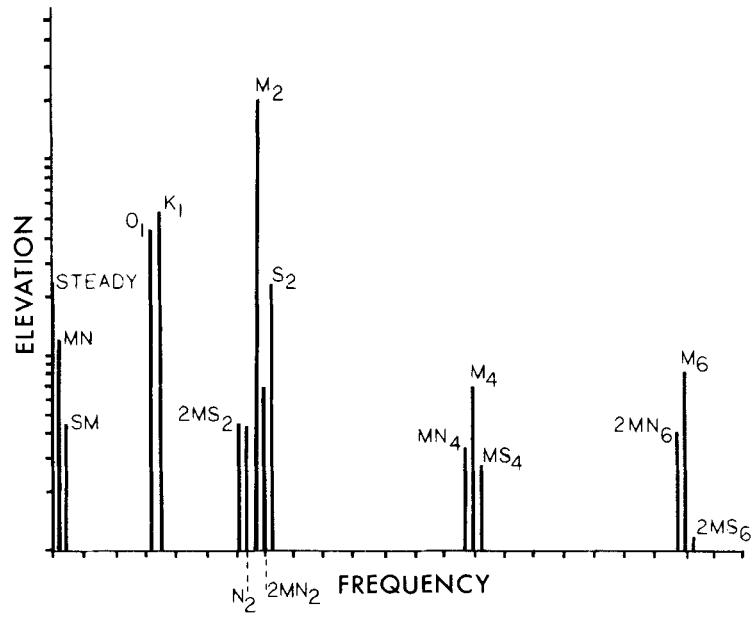

Figure 2. A typical spectrum of harmonic elevation responses within a shallow water estuary showing major astronomical and shallow tide constituents

independent of frequency spacing and resolution. Thus the efficiency of the least-squares harmonic analysis stems from its *a priori* knowledge of the frequency content of the tidal spectrum (a standard assumption in tidal analysis procedures), in addition to the associated very low number of required time sampling points. It is noted that the method of least-squares is essentially identical to specialized applications of Fourier methods which are frequency content selective.[19]

The harmonic least-squares (LSQ) method's ability to extract extremely closely and irregularly spaced frequency information in a very efficient manner makes it the ideal method for the analysis of tidal records. The method has been used extensively in the harmonic analysis of time history records of field-measured tidal elevations. The method is even better qualified for the analysis of analytically generated harmonic responses and non-linear forcing histories, since the signals are guaranteed to be purely harmonic, containing only the exact predictable frequencies associated with a given set of astronomical and shallow water tidal forcing frequencies (i.e. there are no non-tidal forcings). Furthermore, in the analytical generation of these time histories the distribution and length of record of the time sampling points can be conveniently controlled such that optimal accuracy results for a given number of time sampling points.

In order to harmonically decompose a time history record with values $f(t_k)$ at time sampling points t_k, $k=1, M$, and with known frequency content ω_j, $j=1, N$, the following harmonic series is used for the least-squares procedure:

$$g(t)=\sum_{j=1}^{N}(a_j\cos\omega_j t+b_j\sin\omega_j t), \tag{23}$$

where a_j and b_j are the unknown harmonic coefficients. The sums of the squared errors at all sampling times between the fitting function $g(t_k)$ and the function being approximated, $f(t_k)$, is

$$E=\sum_{k=1}^{M}\left(\sum_{j=1}^{N}(a_j\cos\omega_j t_k+b_j\sin\omega_j t_k)-f(t_k)\right)^2. \tag{24}$$

The error minimization is accomplished by setting equal to zero the partial derivatives of E with respect to each of the coefficients a_j and b_j, resulting in

$$\sum_{j=1}^{N}\left[\left(\sum_{k=1}^{M}\cos\omega_j t_k\cos\omega_i t_k\right)a_j+\left(\sum_{k=1}^{M}\sin\omega_j t_k\cos\omega_i t_k\right)b_j\right]=\left(\sum_{k=1}^{M}f(t_k)\cos\omega_i t_k\right),\quad i=1,N, \tag{25a}$$

$$\sum_{j=1}^{N}\left[\left(\sum_{k=1}^{M}\cos\omega_j t_k\sin\omega_i t_k\right)a_j+\left(\sum_{k=1}^{M}\sin\omega_j t_k\sin\omega_i t_k\right)b_j\right]=\left(\sum_{k=1}^{M}f(t_k)\sin\omega_i t_k\right),\quad i=1,N. \tag{25b}$$

This leads to a symmetrical system of $2N$ simultaneous linear equations

$$\mathbf{M}_{\mathrm{LSQ}}\mathbf{A}=\mathbf{F}_{\mathrm{LSQ}}, \tag{26}$$

where

$\mathbf{M}_{\mathrm{LSQ}}$	fully populated least-squares (LSQ) matrix
$\mathbf{A}$	vector of unknown coefficients a_j, b_j
$\mathbf{F}_{\mathrm{LSQ}}$	LSQ signal vector.

Steady-state components in the signal being analysed simply correspond to a frequency equal to zero in the harmonic analysis series (23). This eliminates one row and one column from the matrix $\mathbf{M}_{\mathrm{LSQ}}$ and reduces (26) to a system of $2N$-1 equations. In addition, use of a central time origin with M evenly spaced points Δt time units apart (M must now be an odd integer) allows (26) to be simplified and separated into two smaller subsystems of equations: one fully populated subsystem of N equations for the unknown cosine coefficients a_j which may be expressed as

$$\mathbf{M}_{\text{C-LSQ}}\mathbf{a}=\mathbf{F}_{\text{C-LSQ}}, \tag{27a}$$

where

$$M_{\text{C-LSQ}}(i,j)=\frac{\sin\frac{1}{2}M(\omega_i-\omega_j)\Delta t}{M\sin\frac{1}{2}(\omega_i-\omega_j)\Delta t}+\frac{\sin\frac{1}{2}M(\omega_i+\omega_j)\Delta t}{M\sin\frac{1}{2}(\omega_i+\omega_j)\Delta t}, \tag{27b}$$

$$F_{\text{C-LSQ}}(i)=\frac{2}{M}\sum_{k=-(M-1)/2}^{k=(M-1)/2}f(k\Delta t)\cos\omega_i k\Delta t; \tag{27c}$$

and one fully populated subsystem of $N-1$ equations for the unknown sine coefficient b_j:

where

$$\mathbf{M}_{\text{S-LSQ}}\mathbf{b}=\mathbf{F}_{\text{S-LSQ}}, \tag{27d}$$

$$M_{\text{S-LSQ}}(i,j)=\frac{\sin\frac{1}{2}M(\omega_i-\omega_j)\Delta t}{M\sin\frac{1}{2}(\omega_i-\omega_j)\Delta t}-\frac{\sin\frac{1}{2}M(\omega_i+\omega_j)\Delta t}{M\sin\frac{1}{2}(\omega_i+\omega_j)\Delta t}, \tag{27e}$$

$$F_{\text{S-LSQ}}(i)=\frac{2}{M}\sum_{k=-(M-1)/2}^{k=(M-1)/2}f(k\Delta t)\sin\omega_i k\Delta t. \tag{27f}$$

It is noted that for diagonal positions the first part of the expressions given for both $M_{\text{C-LSQ}}$ and $M_{\text{S-LSQ}}$ reduce to unity.[18]

Since the LSQ matrix (or LSQ submatrices) does not specifically require values of $f(t)$, it need only be generated and triangularized once in order to analyse any of a number of time history signals with the same frequency content. The vector $\mathbf{F}_{\mathrm{LSQ}}$ must however be reset for each time history signal being harmonically analysed. The vector $\mathbf{A}$, which contains the harmonic coeffi-

cients being sought, may then be solved for using the triangularized form of $\mathbf{M}_{LSQ}$. Setting up $\mathbf{F}_{LSQ}$ involves of the order of $O(MN)$ operations and solving for $\mathbf{A}$ involves roughly $O(N^2)$ operations when $\mathbf{M}_{LSQ}$ is in its triangularized form. These operations must be performed for every nodal point at every cycle of the iterative process. In addition the nodal time history values $f(t_k)$, which for our case are the components of the various non-linear load vectors, must be generated at every node for each of the M time sampling points. It is therefore clear that we want to keep the number of time sampling points to an absolute minimum.

For a time history signal for which the entire frequency content is both known and used in the harmonic fitting series, the number of time sampling points required to find (back) the precise signal equals twice the number of frequencies in the signal. This ensures that all the equations in (26) will be linearly independent, providing that no two sampling times are identical nor that two sampling times fall at the same location relative to the overall period of the signal being sampled. The fact that, barring round-off errors, the reproduction of the signal is precise may be inferred by noting that (25) becomes an identity if $f(t)$ is substituted by the original harmonic generating signal.

However, round-off can severely undermine the accuracy of the LSQ procedure. Since, as is noted for (25), the contributions to the components of $\mathbf{M}_{LSQ}$ are all of the same order, the $\mathbf{M}_{LSQ}$ matrix does not exhibit the classical ill-conditioning problems associated with using the least-squares minimization procedure in conjunction with polynomial fitting functions (i.e. Hilbert matrix). Nonetheless, $\mathbf{M}_{LSQ}$ may in general be severely ill-conditioned for a given set of frequencies and time sampling points. The origins of this potential ill-conditioning are most readily seen by examining the structure of the LSQ submatrices for the central time origin case. When either $\frac{1}{2}(\omega_i-\omega_j)\Delta t$ or $\frac{1}{2}(\omega_i+\omega_j)\Delta t$ are in the neighbourhood of or equal to zero, or an integer multiple of π radians, the denominators of the associated terms in the LSQ submatrices given by (27b) and (27e) will be very small (even when the number of time sampling points, M, is very large). Since all numerators in (27b) and (27e) vary between zero and unity, these small denominators result in off-diagonal terms in the matrix which are very large compared with unity. Since the diagonal terms are typically of $O(1)$, this then will lead to very poorly conditioned LSQ submatrices.

However, by carefully selecting the time sampling point spacing Δt, we can avoid ill-conditioning and in fact control the degree of diagonal dominance of the LSQ submatrices. This selection process is based on finding Δt such that the argument of the sine function in the denominators of (27b) and (27e), $\frac{1}{2}(\omega_i \pm \omega_j)\Delta t$, is kept as close to $\pi/2+n\pi$ as possible (where n is any integer). Thus we wish to find a Δt which maximizes p in the following inequality for all frequencies in the signal:

$$\frac{1}{2}-\frac{1}{p}+n<\frac{1}{2\pi}(\omega_i\pm\omega_j)\Delta t<\frac{1}{2}+\frac{1}{p}+n, \tag{28}$$

where n is any integer and p is any real number. The Δt values which result are typically quite large. For cases which we have examined, Δt ranged anywhere from $\frac{1}{2}$ to 8 days, depending on the frequency content of the signal. It is stressed that even seemingly small deviations from the selected optimal values of Δt can lead to low p values and thus very poorly conditioned LSQ submatrices.

Once an optimal Δt value has been found, we can monotonically increase the value of all denominators in the LSQ submatrices by increasing the number of time sampling points, M. Increasing M will result in an overall steady increase in diagonal dominance ratios, although certain select ranges of M lead to especially high ratios compared with those achieved by other nearby values. These optimal M ranges correspond to values of M for which the numerators of

the critical terms in the LSQ submatrices will be small. It is noted that since we have fixed Δt, increasing the number of time sampling points corresponds to increasing the sampling period T_S.

The sampling periods T_S, which correspond to values of Δt and M that result in well-conditioned diagonally dominant matrices, are typically equal to or greater than the period of modulation of the signal. The period of modulation of a signal is obtained by examining its frequency content and selecting the maximum value of all periods or synodic periods of the harmonic components contained in the signal. The synodic period describes the period of beating of two closely spaced frequencies and is computed as

$$T_{SYN} = \frac{2\pi}{\omega_i - \omega_j}. \tag{29}$$

Even though the described procedures typically require relatively few time sampling points to achieve desirable LSQ submatrices, the time sampling periods T_S will in general be very large since the corresponding Δt values are large, usually well in excess of a day. The concept of using large and very specific Δt values in order to reduce computational effort is not new and has previously been applied in tidal field data analysis (e.g. Miyazaki[20]), although not to the extent and with the flexibility possible with our analytically generated signals. Finally it is noted that for signals with typical tidal frequencies and for which the entire frequency content is used in the sampling series, the $(\Delta t, M)$ pair used need only achieve diagonal dominance and a strongly diagonally dominant LSQ matrix is not necessary. Under these circumstances the input signal can be exactly recuperated (to within machine accuracy), often using an M value equal to only about two to three times the number of frequencies in the input signal.

The forcing signals generated by the non-linear terms are such that energy is transferred indefinitely to overtide and compound tide frequencies. The new frequencies which are generated as a result of the non-linear interaction of the various forcing tides through the friction terms appear simultaneously at the second cycle of the non-linear iterative solution procedure. The finite amplitude and convective acceleration terms tend to progressively spread energy to more frequencies as the iteration advances. However, the amount of energy transferred to higher-order harmonics becomes increasingly insignificant. Since it is neither possible nor meaningful to attempt to consider all the frequencies that energy is spread to, the harmonic series representing the non-linear forcings must be truncated, which establishes an order of accuracy for the harmonic analysis.

Neglecting frequencies which are contained in the input signal in the LSQ procedure no longer allows the input harmonics to be recuperated exactly. Errors in the sampling series (23) are now minimized in the true least-squares sense and an increase in the number of sampling points beyond the $M = 2N$ points will be necessary. In general the extent of the error introduced by working with truncated sampling series depends on the distribution and spacing of the harmonics in the input and sampling signals, the relative magnitude of the amplitudes of the neglected harmonics with respect to those being sampled and the noise present in the signal. In our analytically generated signals, noise will not be a factor influencing the accuracy of the results, since these signals are purely harmonic (with the exception of round-off in the input signal which is of no consequence). The only source of significant error in the LSQ analysis of our generated non-linear signals is the influence of the constituents omitted from the sampling series. Assuming that the LSQ submatrices are now strongly diagonally dominant, the error δa_i for a constituent a_i due to an omitted constituent a_{N+1} may be approximated as[18,21]

$$\delta a_i = \frac{\sin \frac{1}{2} M(\omega_i - \omega_{N+1})\Delta t}{M \sin \frac{1}{2}(\omega_i - \omega_{N+1})\Delta t} a_{N+1}. \tag{30}$$

Thus the error introduced depends on both the amplitude of the missing constituents, a_{N+1}, as well as on the magnitude of the hypothetical term which would exist in the LSQ submatrix if we had included this $(N+1)$th constituent in our sampling series (i.e. $M_{\mathrm{LSQ}}(i, N+1)$).

Hence an accurate solution for a given constituent can only be achieved if the products of the terms in the hypothetical LSQ matrix (which corresponds to missing constituents) with the missing constituents themselves are small when compared with the constituent being computed. This criterion, of course, would be met if our time sampling structure were such that the hypothetical LSQ matrix which includes all frequencies in the input signal was very strongly diagonally dominant. However, since a theoretically infinite number of frequencies exist in the non-linear forcing signals which we are analysing, this criterion is impossible to achieve. The best course of action is to carefully consider a limited number of frequencies and attempt to minimize the analysis errors by adhering to the following procedure.

First we must ensure that no significant harmonics are neglected in the sampling series. Significant here implies that all harmonics which exist in the input signal, which are larger than the smallest harmonic which we want to extract from our input signal, should be included in our sampling series. Thus we define N constituents of interest for which the LSQ analysis will be performed. These constituents typically correspond to constituents within the threshold of possible interest for our flow computations. The next step is to generate a secondary sequence of Q frequencies with associated amplitudes smaller than the N harmonics included in our sampling series but which we suspect have a large enough product $M_{\mathrm{LSQ}}(i, j)a_j$ for $i=1, N$; $j=N+1, Q$ to influence any of our N constituents of interest. We now find a $(\Delta t, M)$ pair such that we obtain a sufficiently strong diagonally dominant hypothetical LSQ matrix for our long list of $N+Q$ frequencies. Therefore the errors associated with our actual N-constituent LSQ analysis due to the Q missing frequencies will be small compared with the amplitudes of the constituents being analysed. It is noted that the actual extent of these errors can be controlled by adjusting the degree of diagonal dominance.

Finally we note that there is always the possibility that we have neglected a number of 'hidden' constituents, beyond the $N+Q$ constituents, which potentially could lead to significant errors. In order to check for this possibility and furthermore to obtain a measure of accuracy for each constituent actually analysed, we follow a procedure described by Godin.[21] Godin's procedure involves harmonically analysing R consecutive sequences of signals each of length $T_S=\Delta t M$ and then comparing the results with a 'long' signal of length $RT_{\mathrm{sample}}=\Delta t R M$ (made up of the R signals of length T_S). Since the same time step Δt is being used in the large analysis and since RM time points are used, the diagonal dominance will be much greater and the associated analysis errors much less than for the shorter M-point analysis. The variability in results of the M-point analyses compared with the results of the long analysis will give an excellent indication of the errors for each analysed constituent and furthermore will give an indication of whether we neglected to account for some troublesome hidden constituents. If the errors for certain analysed constituents are unacceptable, we can always increase the diagonal dominance of our hypothetical LSQ matrix for the $N+Q$ constituents. If we suspect the existence of important hidden constituents, we can attempt to find them and include them in our $N+Q$ analysis and minimize their interference.

We found that as a rough guideline for typical shallow water tidal estuary computations (with up to five astronomical and 40 overtide and compound tide constituents included in the non-linear generating series) the number of time sampling points needed to produce sufficiently accurate results varied roughly between four and ten times the number of frequencies, providing that Δt was properly selected and that no frequencies with significant associated amplitudes existing in the input signal were neglected. Since the time steps Δt are typically quite large (e.g. up

to 8 days), this allows for a large sampling period T_S (e.g. 10 years) while using very few time sampling points (e.g. 400). If we applied standard LSQ methods, which do not optimize the selection of the time step and instead simply use $\Delta t = 1$ hour, the same sampling period would require at least 100 times more time sampling points and even then would not necessarily lead to diagonally dominant matrices nor accurate results. Thus the economy and accuracy realized with our tailoring of the LSQ procedure are outstanding and are only possible due to the flexibility we have in analytically generating our signals at any point in time.

Iterative stability and convergence

The iterative stability of every scheme which solves a system of simultaneous non-linear algebraic equations through direct iteration is dependent on the relative importance and character of the terms on both the right-hand and left-hand sides of the system of equations. For the long tidal waves propagating in a typical shallow coastal embayment, the non-linear friction terms have the most pronounced effect of any of the non-linearities on the dynamics of all the tides. This is due in part to the effect of the friction terms on the responses at the dominant frequency. We note that friction becomes especially important in very shallow embayments with rapid velocities. Let us examine the manner in which the non-linear friction term distributes energy to other frequencies. We consider the bottom friction term for a one-dimensional case and approximate the finite amplitude term by a Taylor series expansion

$$c_f \frac{1}{h+\eta}|u|u \simeq c_f \frac{1}{h}|u|u - c_f \frac{\eta}{h^2}|u|u + \ldots . \tag{31}$$

Assuming that only one astronomical tide exists upon the first cycle of iteration, we have an initial response at only the forcing frequency ω_1 of

$$u = \hat{u} \cos \omega_1 t. \tag{32}$$

Substituting into the dominating term of the Taylor series approximation for friction and performing a Fourier expansion, we find that the non-linear forcing will be

$$c_f|u|u \simeq c_f \hat{u}^2(0{\cdot}8488 \cos \omega_1 t + 0{\cdot}1698 \cos 3\omega_1 t - 0{\cdot}0242 \cos 5\omega_1 t + \ldots). \tag{33}$$

Hence there are forcing terms at all the odd harmonics of the forcing frequency ω_1. Equation (33) indicates that for the case of a single astronomical forcing tide the major portion of the harmonically decomposed friction term is distributed to the main astronomical forcing frequency itself. Subsequent cycles of the iterative process will still only generate forcings at the same set of frequencies indicated in (33) and the feedback from the overtide harmonics into the main frequency component at ω_1 will not be significant. We note that the $\eta h^{-2} c_f|u|u$ term of (31) will generate even harmonics (including zero frequency) in the same way that $c_f|u|u$ generated odd harmonics. However, the relative magnitude of the forcings will be much smaller due to the ratio η/h and furthermore will not involve the forcing frequency ω_1.

It can also be shown that for the case of several astronomical forcing tides the dominant tidal frequency (typically the M_2) will still have the largest forcing contribution from the harmonically decomposed non-linear friction term. The magnitude of the non-linear forcing at the dominant frequency will be similar to the forcing which will result when only the dominant astronomical tide is considered. Hence the harmonic friction term at the dominant frequency may be approximated quite well as a linearized friction term. We recall that a spatially varying linearized friction factor λ was incorporated on both sides of the momentum equations earlier. Thus the

iteration occurs about a right-hand-side loading term which equals the difference between a linearized friction term and the fully quadratic friction term.

Proper estimation of λ is essential for rapid convergence of the non-linear scheme. The best convergence rate is achieved by specifying nodal values of λ which somewhat overestimate the actual harmonic non-linear friction term at the dominant frequency. We found that if λ underestimated the non-linear friction the process was divergent, whereas if λ were overestimated excessively convergence rates would be very slow. This then suggests that we first estimate λ to match the actual non-linear friction term at the dominant frequency and then multiply it by a relaxation factor. The optimal relaxation factor was found to be approximately equal to 1·5, which results in nodal values of λ being overspecified by a factor of about 1·5 compared with the actual harmonic component of the fully non-linear friction term at the dominant frequency at convergence. This procedure results in the linear portion of $\hat{\mathbf{P}}^{\mathrm{nl}}_{\Delta-\mathrm{fric}_j}$ exceeding the non-linear portion at almost all frequencies, ensuring positive loadings $\hat{\mathbf{P}}^{\mathrm{nl}}_{\Delta-\mathrm{fric}_j}$. This is in fact what controls the stability of the iterative scheme.

Hence optimal convergence rates are achieved by first obtaining good estimates for the nodal values of the linearized friction factor λ and then relaxing these estimates. A convenient way to obtain a good local estimate for linear friction λ is to update it for a number of cycles using nodal values of c_f and amplitudes of velocity responses generated at the dominant frequency. Since the dominant tide is typically not substantially affected by other smaller astronomical constituents and especially not by shallow water constituents, an excellent estimate of the dominant response can be obtained by considering only the dominant response for a number of cycles while updating λ in the way described. Le Provost and Rougier[9] apply this same type of iterative technique to obtain a quite accurate response at the dominant tidal frequency which they then use in their perturbation computations to drive the shallow water harmonics.

Hence at each of the initial linear iterations performed for only the dominant frequency we update λ as follows:

$$\lambda^{(i+1)} = 0{\cdot}5(\lambda^{(i)} + 0{\cdot}8488 c_f |\hat{u}_d^2 + \hat{v}_d^2|^{0{\cdot}5}), \tag{34}$$

where $\lambda^{(i)}$ represents a nodal linear friction coefficient at cycle i which allows the approximation of the harmonic friction term at the dominant frequency; 0·8488 represents the coefficient of the leading term of the Fourier series expansion for the non-linear friction term in (33): $\hat{u}_d$, $\hat{v}_d$ are the nodal amplitudes of velocity at the dominant frequency at cycle i. The averaging between the value of λ at the present cycle and the term involving c_f and velocities minimized overshoot and undershoot problems that occur with this type of iterative approximation. This procedure typically led to a good stable value of λ and associated dominant responses in about five linear cycles, regardless of the initial user-specified values of λ which are used in the first cycle of iteration. We stress that these first five or so cycles of the iteration only involve one frequency component and no generation or harmonic decomposition of any non-linear forcing vectors. Thus the linear core solution is run only once at each of these initial linear start-up cycles and values of λ are updated using computed responses at the dominant frequency.

After these initial purely linear iterations, we relax the λ factors and proceed with non-linear iterations by considering the non-linear terms and all frequencies which demonstrate themselves to be significant. No further modifications of the linearized friction factor λ are implemented. We note that by relaxing λ only after the end of the last fully linear cycle we speed up our iterative process, since in this way the non-linear iteration starts with good estimates of responses at the dominant tidal frequency. We recall that these dominant responses are largely responsible for driving the shallow water tides either due to the interaction with themselves, other astronomical responses or shallow water tidal responses which have previously been generated. We therefore

also eliminate substantial overshoot and undershoot problems in our non-linear iterative cycles which could have otherwise significantly decreased convergence rates.

Let us now examine the effect of the finite amplitude terms in the continuity equation on the iterative stability of our scheme. As mentioned earlier, the finite amplitude term distributes its loading progressively as the iteration proceeds. A forcing tide with a response at ω_1 generates a non-linear finite amplitude forcing at steady state and $2\omega_1$. The second cycle of the non-linear iteration produces forcings at steady state, ω_1, $2\omega_1$, $3\omega_1$ and $4\omega_1$. However, the non-linear forcings at ω_1, $3\omega_1$ and $4\omega_1$ are due to the interaction of the relatively small responses at steady state and $2\omega_1$, with the more significant responses at ω_1 or with themselves (i.e. one or both parts of the product $\hat{u}_i\hat{\eta}_j$, where these are the harmonic response amplitudes associated with the various frequencies, will be from responses at steady state or $2\omega_1$). Thus the non-linear forcings will be much smaller for these second non-linear cycle harmonics compared with the first cycle harmonics, steady state and $2\omega_1$, which resulted from the ω_1 constituent interacting with itself. Hence the character of the energy distribution due to the non-linear interaction which occurs through the finite amplitude term is distinctly different from the friction term in that the most important effects are at frequencies other than the initial forcing frequency and that the distribution of energy progresses with each iteration. We note that the dominant frequency will not be substantially affected by the finite amplitude terms. Furthermore, as a result of the dominant responses having already stabilized at the beginning of the non-linear cycling, the finite amplitude term also spreads energy to other frequencies without any overshoot/undershoot problems.

The stability associated with the iterative treatment of the finite amplitude term may be inferred from Lamb[22] who shows that there are theoretical limitations for iterative schemes for this term which relate to the relative size (with respect to the wavelength) of the estuary. Lamb shows that when solving for the case of an open ended canal, the solution obtained by treating the finite amplitude term by successive approximations will be unstable if $2\pi(a/h)(x/\lambda)$ is not small, where x equals the length of the canal, a equals the amplitude of the wave and λ equals the wavelength. Even though the same difficulty does not necessarily occur for the case of a closed-ended canal, the criterion may be viewed as being indicative of potential instabilities. This criterion will be largest in very shallow water when the associated wavelength of a given tidal component will be the shortest and the ratio a/h will be the largest. Hence the shallower the water depth and the higher the amplitude of the tide, the smaller will be the maximum allowable theoretical dimension of the basin for iterative stability. However, in general the criterion is well met for typical coastal geometries owing to the long wavelengths associated with tidal components. Therefore unless dealing with very shallow and large coastal seas, this potential instability will not be a limitation of the method.

The convective acceleration terms are similar to the finite amplitude terms in the continuity equation in the way they distribute energy through the iterative solution procedure. Convective acceleration terms become important only in rapidly varying geometries such as narrow tidal inlets connecting a wide embayment to the open ocean. We have not investigated the stability of the iterative treatment of these terms in the case of strongly convecting flows. It is noted that for these cases eddy viscosity terms would most likely also play an important role and would have to be taken into consideration.

So far we have looked at general factors which control stability and some ways of improving convergence rates. Let us now address the question of the point at which we can consider the solution to have converged. Obviously the computational effort of TEA-NL is directly related to the total number of iterative cycles that need to be run. When determining the degree of accuracy which the iteration process should achieve, we should consider a number of factors.

First of all there is an order of accuracy associated with the FE method used for the spatial discretization of the governing equations. This spatial accuracy depends on the grid size and the gradients of the variables relative to the grid size. Furthermore, all numerical schemes solving the linear harmonic shallow water equations exhibit a certain degree of nodal oscillations in the solution computed for elevation and velocity. The nodal oscillations of the PPWE scheme are very well controlled and are dependent on the geometry, depth variation and extent of discretization. The accuracy of the computation is not improved by carrying out the iterative accuracy beyond the estimated amplitude of these nodal oscillations.

Furthermore, the non-linear forcings are generated with elevations and velocities which contain a certain degree of nodal oscillation. We therefore expect some deterioration in the solution achieved at higher-order harmonics. The degree of deterioration depends on the magnitude of oscillation relative to the overall magnitude of forcing (signal-to-noise ratio). Furthermore, it depends on which of the non-linear terms are included in the analysis and their relative importance. Owing to the way in which the finite amplitude and convective terms progressively spread energy to higher harmonics through interactions with the non-linear tides themselves and owing to the fact that derivatives are involved in these terms, a steady deterioration in the quality of the results is seen. Hence as energy is cascaded down to higher-order harmonics, the nodal oscillations increase because the noise in the forcing at each non-linear frequency is somewhat enhanced by the linear computation itself. For the non-linear friction forcings this signal/noise effect is less pronounced, since the forcing term does not include any derivatives of velocity and furthermore because energy is distributed mainly from the major astronomical forcing frequencies to all the non-linear forcing frequencies simultaneously. It is important to consider this noise in the non-linear forcings when determining the convergence achievable at each of the frequencies.

Finally we note that there is an order of accuracy associated with the truncation of the harmonic series used for the resolution of the time dependence of the governing equations. The frequencies taken into consideration are affected to a certain degree by the lack of interaction with the missing harmonics. However, the overall accuracy of the computation by not considering this interaction is no worse than that achieved by not considering these terms in the first place. Thus performing a calculation of the response at a given frequency beyond the estimated percentage of the missing non-linear interaction would not be meaningful. In addition there are errors associated with the LSQ harmonic analysis procedure itself as a result of the required truncation of the sampling series. The degree of accuracy achieved with the harmonic analysis procedure depends on a number of factors previously examined.

The points discussed should be taken into consideration when determining the level of accuracy which the iterative process should achieve. This level is case-dependent and also varies for each of the frequencies for which the calculations are being performed. Program TEA-NL allows the determination of the level of accuracy achieved and the rate of convergence by computing a variety of convergence parameters.

APPLICATION OF THE NON-LINEAR MODEL

As an application of the non-linear model, TEA-NL, we shall examine the behaviour of a variety of non-linear type interactions which occur in a straight closed-ended shallow channel. The FE discretization of the channel is shown in Figure 3. It is 50 km long and 8 km wide and has a depth of 5 m. It is open to the ocean on the left side, where the astronomical tides will be applied as boundary forcings. It is assumed that a sharp depth discontinuity will cause the open ocean

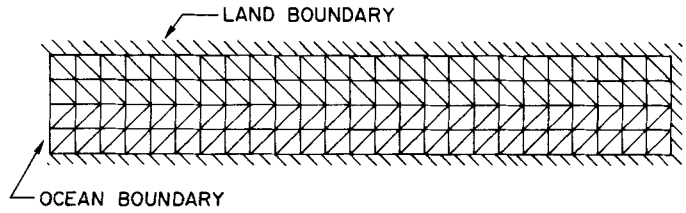

Figure 3. FE discretization of channel geometry

Table II. Runs for non-linear interactions examples

Case	Boundary forcing tides	Non-linearities: Finite amplitude in continuity	Non-linearities: Nonlinear friction	Non-linearities: Finite amplitude in friction term
1	M_2	Yes	No	No
2	M_2	No	Yes	No
3	M_2	No	Yes	Yes
4	M_2	Yes	Yes	Yes
5	M_2, N_2	Yes	Yes	Yes

boundary to fully reflect out of phase any non-linear shallow water tides generated within the channel. Hence all shallow water tides will have zero elevation-prescribed boundary conditions on the open ocean boundary. The cases examined are summarized in Table II.

M_2 astronomical boundary forcing

Let us first examine a series of cases which demonstrate the influence of the non-linearities on those overtides generated as a result of an M_2 boundary forcing tide. Since no other astronomical forcing tides are applied, only overtides are produced and we shall refer to this series of runs (1–4) as overtide cases. An M_2 astronomical forcing tide of 1·0 m with no applied phase shift can generate the overtides listed in Table III. All associated overtide frequencies occur at integer multiples of the M_2 frequency. The LSQ harmonic analysis was applied using a central time origin with 38 evenly spaced time points distributed over the period of modulation of the signal, 12·42 hours. This leads to LSQ submatrices with all off-diagonal terms equal to zero and the ability to harmonically analyse the generated non-linear signals with essentially no errors for any of the constituents.

Case 1. The effect of finite amplitude in the continuity equation. First let us examine the influence on the generation of overtides of the finite amplitude term in the continuity equation. For Case 1 we specify a linearized friction factor of $\lambda = 0{\cdot}00270$ and the non-linear friction term is turned off. The linear friction factor has been chosen to give the same channel-averaged response in M_2 elevation as Cases 2–5 which all have non-linear friction turned on and specified as $c_f = 0{\cdot}005$. In fact for this case we do not iterate in the purely linear fashion described in the previous section to update estimates for λ based on M_2 responses and c_f values, but we simply

Table III. List of frequencies used for M_2 overtide cases (Cases 1–4)

Tide	Frequency (rad s^{-1})	Period (h)	Synodic period (days)
Steady	0·00000000000	—	0·00
M_2	0·00014051892	12·42	0·52
M_4	0·00028103783	6·21	0·52
M_6	0·00042155675	4·14	0·52
M_8	0·00056207567	3·11	0·52
M_{10}	0·00070259459	2·48	0·52
M_{12}	0·00084311350	2·07	0·52
M_{14}	0·00098363242	1·77	0·52
M_{16}	0·00112415134	1·55	0·52
M_{18}	0·00126467025	1·38	—

work with a globally constant user-specified value. We note from curves 1 in Figures 4(b) and (c) that the M_2 component elevation amplitude is increasingly damped and phase lag increases as we progress further into the channel.

Table IV lists the channel-nodal-averaged amplitudes of the harmonic non-linear finite amplitude forcing components for the continuity equation, $\bar{P}_\eta$, and the non-linear friction forcing components for the momentum equation, $\bar{P}_U$ (i.e. the non-linear portion of $\hat{\mathbf{P}}^{\mathrm{nl}}_{\Delta-\mathrm{fric}_j}$), at the various overtide frequencies. The table indicates that the most significant non-linear continuity equation loadings occur at the steady state and M_4 harmonics. The response in elevation at steady state is somewhat larger than that at M_4, as can be seen by examining curves 1 in Figures 4(a) and (d). A much smaller non-linear forcing occurs at M_2, although the effect on the M_2 response is negligible compared with that of the boundary forcing. Finally we note that the forcings and associated responses at higher harmonics (M_6, M_8, M_{10}) become increasingly smaller. As was

Table IV. Basin-averaged harmonic non-linear forcings and responses for M_2 astronomical boundary forcing cases for various non-linear interactions (numbers given to two significant figures)

Case	Variable	Steady	M_2	M_4	M_6	M_8	M_{10}
1	$\bar{P}_\eta$	39	12	62	6·1	0·84	0·12
	$\bar{P}_U$	0	0	0	0	0	0
	$\bar{\eta}$	0·037	0·69	0·022	0·0016	0·00017	0·000021
2	$\bar{P}_\eta$	0	0	0	0	0	0
	$\bar{P}_U$	10^{-7}	1650	10^{-7}	150	10^{-7}	80
	$\bar{\eta}$	10^{-11}	0.69	10^{-11}	0·035	10^{-11}	0·013
3	$\bar{P}_\eta$	0	0	0	0	0	0
	$\bar{P}_U$	54	1650	61	150	13	79
	$\bar{\eta}$	0·028	0·69	0·015	0·034	0·0026	0·013
4	$\bar{P}_\eta$	41	15	60	7·6	6·5	2·6
	$\bar{P}_U$	150	1640	190	120	50	67
	$\bar{\eta}$	0·076	0·69	0·047	0·029	0·011	0·010

noted earlier, this is due to the fact that these higher-order harmonics appear as a result of the interaction of weaker overtide responses with the M_2 constituent or with themselves, resulting in progressively rapidly decreasing forcings and associated responses for higher-order harmonics. Responses in elevation amplitude and phase for steady through M_6 are all shown as curves 1 in Figure 4. Finally we note that had the linear friction coefficient λ been specified as zero, then the M_2 response would have increased through the channel without any phase lag. Furthermore, the steady-state response would have been zero (due to the phase difference of $\pi/2$ between elevation and velocity responses) and the M_4 and M_6 responses would all have been larger due to the increased M_2 amplitudes and would also have no phase lag.

Case 2. Non-linear friction with no finite amplitude effects. We now look at the effects of a non-linear friction term with no finite amplitude effects in either the continuity or the momentum equations. Hence the shallow water equations (1) and (2) are simplified by assuming $h+\eta=h$. Table IV shows that non-linear forcings for the momentum equation occur at all odd harmonics (M_2, M_6, M_{10}, etc.) and virtually no forcing nor response occurs at the even harmonics (steady, M_4, M_8). This is consistent with the discussion earlier. We note that the even-harmonic forcings are within the error level of the LSQ analysis procedure. The major forcing of the non-linear friction term with an M_2 forcing tide is on the M_2 component itself. Although the channel-averaged M_2 response is the same as Case 1, elevation amplitude and phase are distributed somewhat differently, as indicated in Figures 4(b) and (c). If we had applied the purely linear part of the iteration procedure to obtain estimates for λ in Case 1, the M_2 response for Case 1 would have been essentially the same as for Case 2.

The forcings and responses at odd overtide frequencies do not diminish as rapidly as in Case 1. This is due to the fact that the M_2 tide is directly forcing (by interacting with itself) all these harmonics, as can also be deduced by examining (33). Responses in elevation amplitude and phase for Case 2 for the steady through M_6 components are shown in Figure 4.

Case 3. Non-linear friction with finite amplitude in the momentum equation only. Case 3 considers the effect of including finite amplitude in the momentum but not the continuity equation. Table IV indicates that the forcings and responses at the odd harmonics have remained essentially unchanged compared with Case 2. However, now the finite amplitude part of the friction term causes forcings and responses at the even harmonics which are in general smaller than those at odd harmonics. Comparing the response at the even harmonics generated due to finite amplitude alone (Case 1), we note from Table IV that the non-linear friction terms generate a smaller response at steady and M_4 than the continuity finite amplitude term, but generate a larger response at M_8 (and M_{12}, etc.). This is again due to the fact that it is the M_2 tide that is responsible for the simultaneous forcing of the even harmonics in the case of the friction term with finite amplitude effects included. Responses in elevation for the various frequencies are shown and compared with the other cases in Figure 4.

Case 4. Non-linear friction and non-linear finite amplitude. Case 4 examines the effect of non-linear friction in addition to finite amplitude in both the momentum and continuity equations. We note from Table IV that the averaged non-linear forcings for the continuity equation, $\bar{P}_\eta$, are similar to the case of finite amplitude alone (Case 1) for steady through M_6 and much greater for M_8 and M_{10}. This redistribution of non-linear forcings is explained by the fact that the M_6 response for Case 4 is an order of magnitude larger than for Case 1 due to non-linear friction. This results in increased forcing $\bar{P}_\eta$ at M_8. The same holds true for $\bar{P}_\eta$ at M_{10}. Furthermore, non-linear forcings for the momentum equation have significantly increased at the even harmonics and have

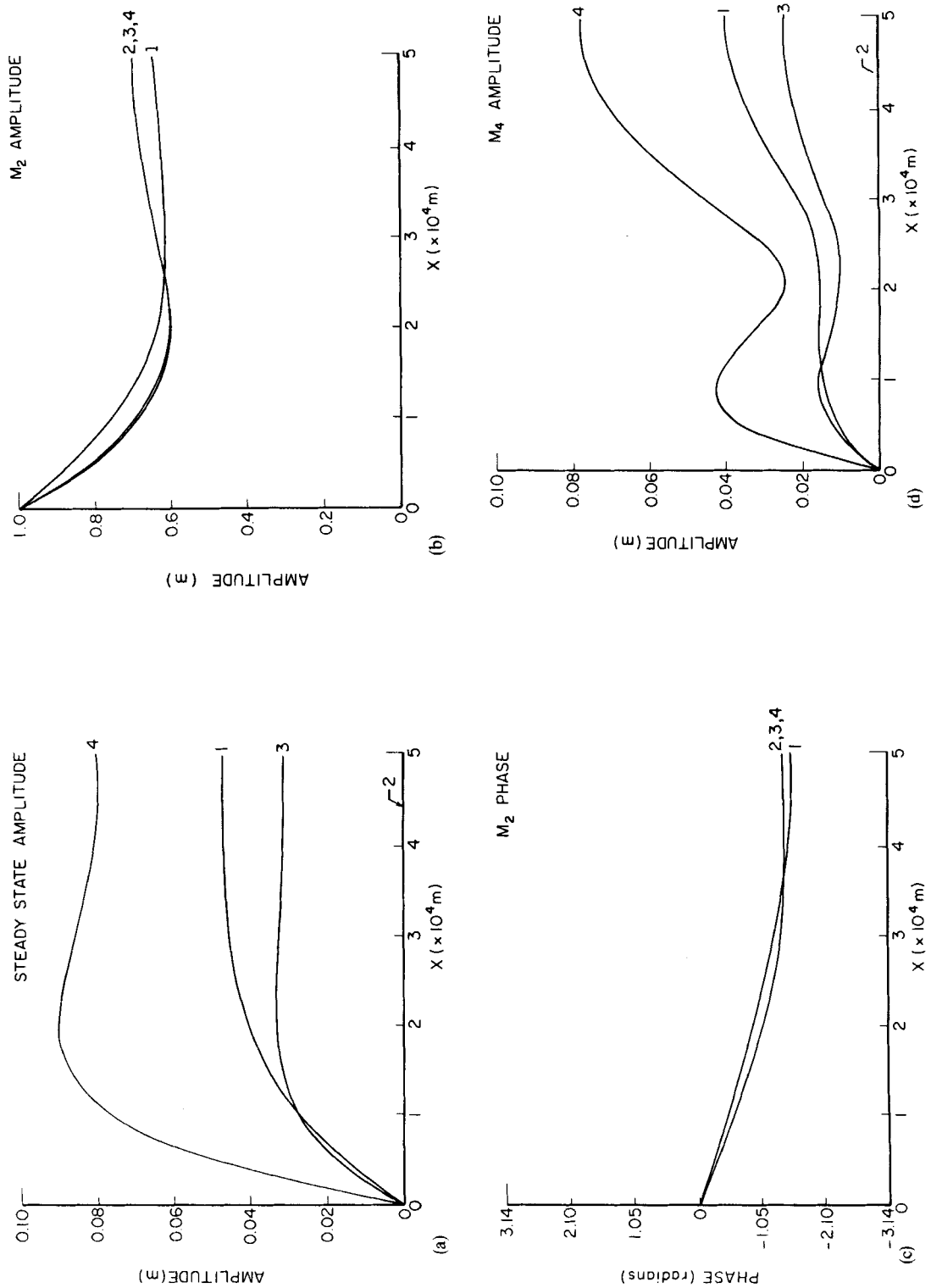
STEADY STATE AMPLITUDE
AMPLITUDE(m)
X (×10⁴m)
(a)
M₂ AMPLITUDE
AMPLITUDE (m)
2,3,4
1
(b)
M₂ PHASE
PHASE (radians)
(c)
M₄ AMPLITUDE
AMPLITUDE (m)
(d)

Figure 4. (a–d)

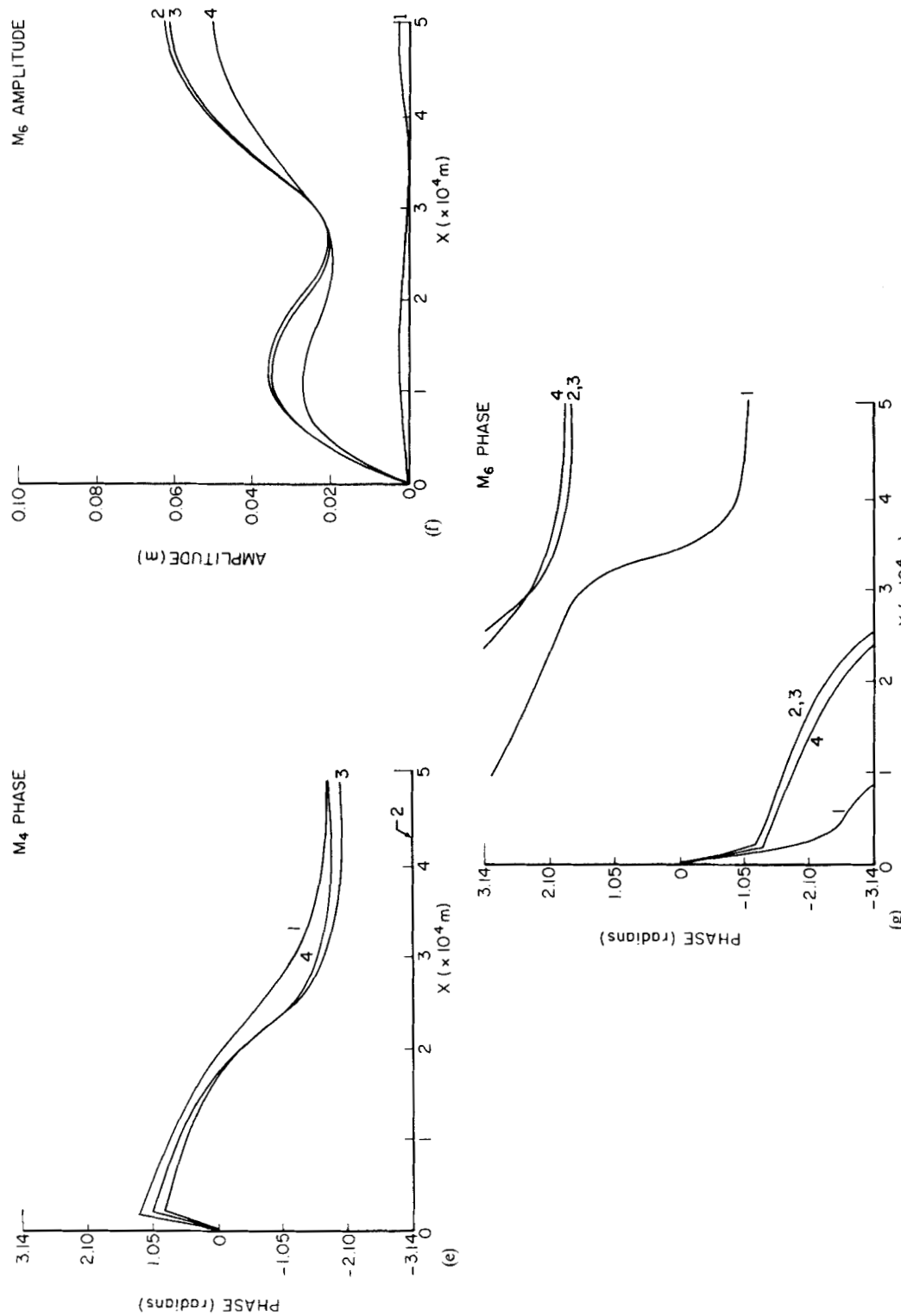

Figure 4. Comparison of elevation amplitude and phase for various overtide cases (Cases 1–4). Response curves are labelled for the case with which they are associated. (a) Steady-state amplitude. (b) M_2 amplitude. (c) M_2 phase. (d) M_4 amplitude. (e) M_4 phase. (f) M_6 amplitude. (g) M_6 phase

been reduced at the odd harmonics. This is due to the reinforcing of continuity finite amplitude and momentum friction effects at even harmonics. The increased responses at these harmonics in turn increase the frictional loadings at the harmonics themselves. A reduction in the M_6 and odd-harmonic momentum non-linear loadings is brought about by a finite amplitude forcing which is partially out of phase from the frictional forcing (see Figure 4(g) to deduce this). Together with a small increase in $\bar{P}_\eta$ at M_6, this reduces the M_6 response and momentum non-linear forcings. The redistribution of non-linear forcings described leads to significantly increased responses at steady, M_4 and M_8 while causing reduced responses at M_6 and M_{10}. The response at M_2 remains virtually unchanged. Elevation responses for Case 4 are shown together with results for Cases 1–3 in Figure 4 for the steady through M_6 constituents.

M_2 and N_2 astronomical boundary forcing

We now examine the non-linear interactions brought about by two astronomical boundary forcing tides. The astronomical forcing constituents selected are the dominant M_2 tide, forcing the open ocean boundary with an amplitude of 1 m, and the N_2 tide, forcing the open ocean boundary with an amplitude of 0·25 m out of phase with respect to the M_2 by 5·934 rad (i.e. lagging the M_2 by almost a full cycle). The overtides and compound tides and their associated frequencies that will be generated through the non-linearities with this M_2–N_2 interaction are listed in Table V. The LSQ harmonic analysis is now applied using the frequencies listed and 97 time sampling points spaced at 13·70196 hours. Thus the sampling period is slightly greater than twice the modulating period for the frequencies under consideration. The minimum diagonal dominance ratio in the LSQ submatrices is 12·8 and the average diagonal dominance is 22·5, while

Table V. List of frequencies used for M_2–N_2 compound tide cases (Case 5)

Tide	Frequency (rad s^{-1})	Period (h)	Synodic period (days)
Steady	0·00000000000	—	0·00
MN	0·00000263920	661·31	27·55
2(MN)	0·00000527840	330·65	0·56
$2NM_2$	0·00013524051	12·91	27·55
N_2	0·00013787971	12·66	27·55
M_2	0·00014051891	12·42	27·55
$2MN_2$	0·00014315812	12·19	0·56
$3NM_4$	0·00027312022	6·39	27·55
N_4	0·00027575942	6·33	27·55
MN_4	0·00027839863	6·27	27·55
M_4	0·00028103783	6·21	27·55
$3MN_4$	0·00028367703	6·15	0·56
N_6	0·00041363914	4·22	27·55
$2NM_6$	0·00041627834	4·19	27·55
$2MN_6$	0·00041891754	4·17	27·55
M_6	0·00042155675	4·14	0·56
N_8	0·00055151885	3·16	27·55
$3NM_8$	0·00055415805	3·15	27·55
$2(MN)_8$	0·00055679726	3·13	27·55
$3MN_8$	0·00055943646	3·12	27·55
M_8	0·00056207566	3·11	0·52
M_{10}	0·00070259459	2·48	—

individual diagonal to off-diagonal term ratios are about five times greater. The resulting error in the harmonic analysis is less than 1% for all significant constituents. Significant constituents for this case were the steady, MN, N_2, M_2, $2MN_2$, MN_4, M_4, $2MN_6$, M_6, $3MN_8$, M_8 and M_{10} constituents. Other constituents were found to have comparatively small non-linear forcing amplitudes and responses.

For this compound tide case (Case 5) finite amplitude and non-linear friction were included. A comparison of basin-averaged non-linear loadings and elevation responses is shown in Table VI. It is noted that forcings and responses for the steady, M_2 and M_4 are very close to those of Case 4. A slight increase in response for the steady and a slight decrease for M_2 and M_4 are indicated in Figures 5(a), (d) and (g), which compare elevation amplitudes for Cases 4 and 5. However, Table VI and Figure 5(i) indicate that a much more significant reduction is brought about in the M_6 forcings and responses.

Compound tidal components listed in Table VI generally exhibited a response of about 50% of that of the adjacent overtide response. Figure 5 indicates that the elevation amplitude response curves of the compound tides show similar form to the adjacent overtides (steady and MN; M_4 and MN_4; MN_6 and M_6). Furthermore, elevation phases for adjacent components were very similar.

Convergence and noise

Convergence was quite rapid in all the cases described. With the exception of Case 1, all cases first performed five purely linear cycles, involving only the M_2 tide, to compute nodal λ values such that λ closely approximates the harmonic non-linear friction forcing at M_2. At the end of the fifth cycle λ values were relaxed by multiplying them by 1·5. For all cases the M_2 amplitudes of elevation and velocity had converged to less than 1% relative change (the average difference between nodal values at two consecutive cycles divided by the average nodal value of the variable at the updated cycle) by the third fully non-linear cycle and all overtide and compound tides with significant computed responses had converged to better than 1% by the end of the seventh or eighth fully non-linear cycle. This convergence was more progressive (i.e. M_4 converged at cycle 5, M_6 at cycle 6, etc.) for Case 1 than for cases which included friction owing to the nature of the energy transfer mechanisms and the amount of energy transferred back to other non-linear forcing tides.

The extent of nodal oscillations increased as energy was spread to higher-order harmonics. The nodal oscillations were markedly the worst at very high harmonics for Case 1 due to the finite amplitude term. They were the best for Cases 2 and 3 with only the friction term being involved in the computations. Furthermore, in these cases the nodal oscillations increased at a much slower

Table VI. Basin-averaged harmonic non-linear-forcings and responses for M_2 and M_2–N_2 astronomical boundary forcings and full non-linear interaction (numbers given to two significant figures)

Case	Variable	Steady	MN	N_2	M_2	$2MN_2$	MN_4	M_4	$2MN_6$	M_6
4	$\bar{P}_\eta$	41	—	—	15	—	—	60	—	7·6
	$\bar{P}_U$	150	—	—	1640	—	—	190	—	120
	$\bar{\eta}$	0·076	—	—	0·69	—	—	0·047	—	0·029
5	$\bar{P}_\eta$	42	17	6·8	16	3·0	26	58	4·8	7·1
	$\bar{P}_U$	160	79	420	1630	42	94	190	45	110
	$\bar{\eta}$	0·079	0·041	0·14	0·68	0·025	0·021	0·046	0·011	0·024

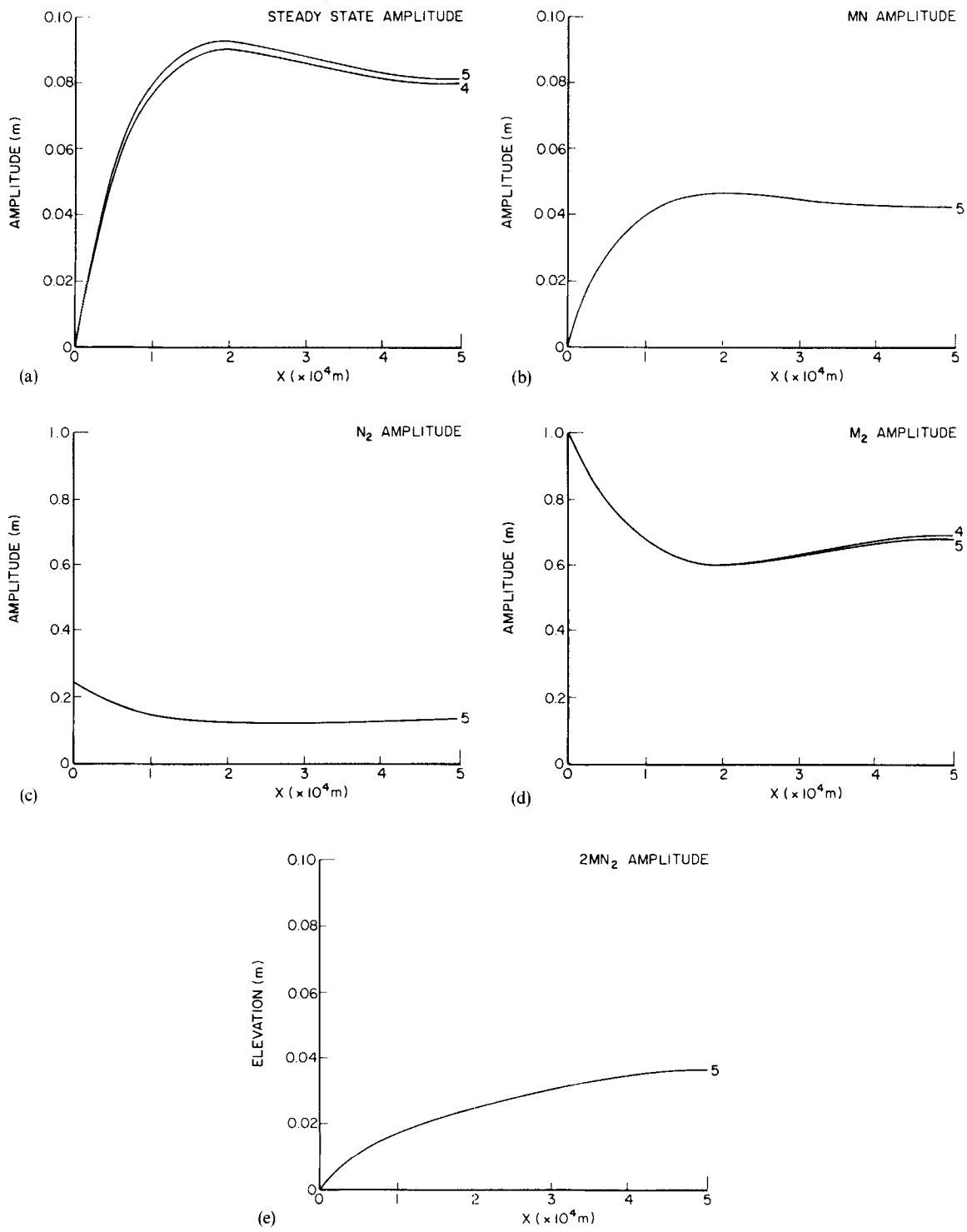
STEADY STATE AMPLITUDE
AMPLITUDE (m)
0.10
0.08
0.06
0.04
0.02
0
0 1 2 3 4 5
X (×10⁴m)
5
4
(a)
MN AMPLITUDE
AMPLITUDE (m)
X (×10⁴m)
5
(b)
N₂ AMPLITUDE
AMPLITUDE (m)
1.0
0.8
0.6
0.4
0.2
X (×10⁴m)
5
(c)
M₂ AMPLITUDE
AMPLITUDE (m)
X (×10⁴m)
4
5
(d)
2MN₂ AMPLITUDE
ELEVATION (m)
X (×10⁴m)
5
(e)

Figure 5. (a–e)

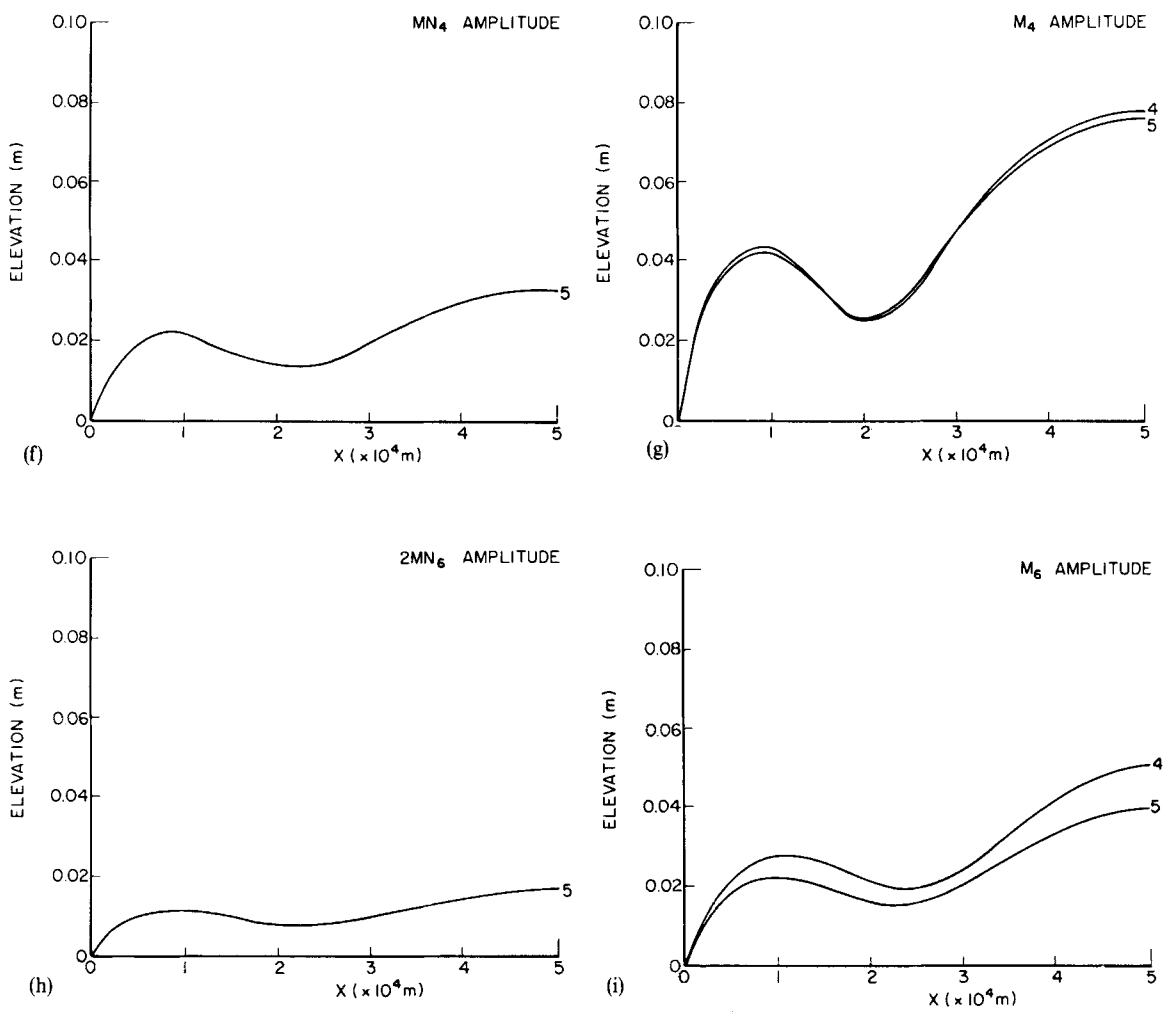

Figure 5. Comparison of elevation amplitude for compound tide runs. (a) Steady-state amplitude. (b) MN amplitude. (c) N_2 amplitude. (d) M_2 amplitude. (e) $2MN_2$ amplitude. (f) MN_4 amplitude. (g) M_4 amplitude. (h) $2MN_6$ amplitude. (i) M_6 amplitude

rate for the higher-order harmonics than for Case 1. Case 4 with both finite amplitude and friction terms has oscillations characterized by features of both Cases 1 and 3. The M_2 tide for Case 4 has a maximum cross-channel relative oscillation in elevation amplitude (cross-channel change divided by elevation values) of 0·04% with a channel-averaged value of 0·002%, while the shallow water constituents typically had a maximum cross-channel oscillation of about 3% with a channel average of the order of 0·1%. For Case 5 the oscillations in the compound tides were slightly greater than in the corresponding adjacent overtides.

Summary

In summary we note that the compound tides are very significant in non-linear shallow water tidal dynamics in terms of their magnitude relative to adjacent overtides and also due to their

effect on certain overtides (e.g. reduction in M_6). Of further interest is that long-period responses are generated both due to overtide type interactions and compound tide type interactions. In particular a significant steady-state set-up is generated which is of the same order of importance as other overtide constituents. Associated with this steady-state set-up are significant outward steady velocities (in amplitude about 8% of maximum M_2 velocity responses) in the front portion of the bay. Furthermore, a long-term-varying MN response with a period of 27·55 days causes a slowly oscillating current which has a peak velocity of about half the steady-state velocity response. Steady-state and other long-term-varying residual tidal circulations will certainly be important for drift velocity and pollutant transport computations.

Finally we note that the overtides of the N_2 tide were insignificant. The order of importance of the shallow water tides for this case is first the overtides of the M_2 tide, then the compound tides due to the M_2–N_2 interaction and finally the N_2 overtides. This is due to the fact that the strongest interactions are represented by the M_2 interacting with itself through the non-linearities and then the major M_2 interacting with other astronomical and shallow water constituents. The interaction of N_2 with itself is not significant.

CONCLUSION

The development of TEA-NL has generated a powerful tool which allows the general investigation of non-linear shallow water tidal dynamics. The iterative nature of the scheme in conjunction with the use of the harmonic least-squares analysis method makes TEA-NL entirely general in the sense that any tidal constituent can be examined and furthermore in that we do not establish *a priori* the importance of the various non-linear interactions as a perturbation scheme would. The simulation of tidal flows in estuaries is quite straightforward and the computation of long-term residual circulations is accomplished simply by studying the low-frequency end of the response spectrum.

TEA-NL incorporates a variety of unique features which include:

(i) A finite element harmonic solution based on the primitive equations which exhibits low spurious spatial oscillations. We note that it is crucial to minimize the spatial noise since high noise/signal ratios would not allow for the correct computation of the non-linear forcings and the solutions at higher-order harmonics would degrade rapidly. The PPWE scheme used to solve the linear harmonic equation in TEA-NL, however, shows excellent control on spatial noise and thus allows for the accurate study of quite high-order harmonics in the shallow water spectrum which have very small responses.

(ii) A least-squares harmonic analysis procedure which readily allows for the harmonic decomposition of signals with closely and unevenly spaced energy in a very economical fashion. Owing to the flexibility we have in analytically generating the required time history signals, we have tailored the least-squares procedure such that we are typically able to reduce the number of required time history points by several orders of magnitude when compared with standard least-squares procedures. In general the least-squares method allows for the forthright inclusion of compound tides which as we have noted are very important to the shallow water tidal dynamics of an estuary. Compound tides influence the M_2 overtides and furthermore their associated responses are significant relative to the adjacent M_2 overtides.

(iii) The components of the harmonic iterative type procedure show a high degree of parallelism and therefore make TEA-NL ideally suited for implementation on the emerging new generation of parallel processing supercomputers. All the CPU time intensive computations for this scheme are extremely amenable to parallel processing. For a typical field application the generation of the time history response is the most CPU time intensive. This is followed by the linear core solution at all N_f frequencies. The LSQ harmonic analysis and the generation of the time history loading from the time history response are significantly less CPU intensive. As is indicated in Figure 2, all of these components of TEA-NL can be processed in a parallel fashion either on a frequency basis or on a nodal basis, leading to significant increases in computational efficiency. In addition the use of supercomputers with a significantly larger virtual memory will increase the efficiency of TEA-NL in that there will no longer be a need to reset and resolve the system matrices for each frequency beyond the first fully non-linear iteration.

A detailed field application to the Bight of Abaco, Bahamas, will be presented in a subsequent paper.

REFERENCES

1. J. J. Dronkers, *Tidal Computations in Rivers and Coastal Waters*, Wiley, New York, 1964.
2. M. Kawahara, K. Hawegawa and Y. Kawanago, 'Periodic tidal flow analysis by finite element perturbation method', *Comput. Fluids*, **5**, 175–189 (1977).
3. C. E. Pearson and D. F. Winter, 'On the calculation of tidal currents in homogeneous estuaries', *J. Phys. Oceanogr.*, **7**(4), 520–531 (1977).
4. C. Le Provost and A. Poncet, 'Finite element method for spectral modelling of tides', *Int. j. numer. methods eng.*, **12**, 853–871 (1978).
5. R. L. Snyder, M. Sidjabat and J. H. Filloux, 'A study of tides, setup and bottom friction in a shallow semi-enclosed basin. Part II: Tidal model and comparison with data', *J. Phys. Oceanogr.*, **9**, 170–188 (1979).
6. A. Askar and A. S. Cakmak, 'Studies on finite amplitude waves in bounded water bodies', *Adv. Water Resources*, **1**(4), 229–246 (1978).
7. M. Kawahara and K. Hasegawa, 'Periodic Galerkin finite element method of tidal flow', *Int. j. numer. methods eng.*, **12**, 115–127 (1978).
8. C. Le Provost, 'A model for prediction of tidal elevations over the English Channel', *Oceanologica Acta*, **4** (3), 279–288 (1981).
9. C. Le Provost and G. Rougier, 'Numerical modeling of the harmonic constituents of the tides, with application to the English Channel', *J. Phys. Oceanogr.*, **11**(8), 1123–1138 (1981).
10. W. Horn, 'The harmonic analysis, according to the least squares rule, of tide observations upon which an unknown drift is superposed', *Third Int. Symp. on Earth Tides*, Trieste, 6–11 July 1959.
11. W. Horn, 'Some recent approaches to tidal problems', *Int. Hydro. Rev.*, **37**(2), 65–84 (1960).
12. J. J. Westerink, J. J. Connor and K. D. Stolzenbach, 'A primitive pseudo wave equation formulation for solving the harmonic shallow water equations', *Adv. Water Resources*, (1988) in press.
13. W. G. Gray and D. R. Lynch, 'On the control of noise in finite element tidal computations: a semi-implicit approach', *Comput. Fluids*, **7**, 47–67 (1979).
14. D. R. Lynch and W. G. Gray, 'A wave equation model for finite element tidal computations', *Comput. Fluids*, **7**, 207–228 (1979).
15. D. R. Lynch, 'Mass balance in shallow water simulations', *Commun. appl. numer. methods*, **1**, 153–159 (1985).
16. A. V. Oppenheim and R. W. Schafer, *Digital Signal Processing*, Prentice Hall Inc., Englewood Cliffs, NJ, 1975.
17. D. E. Newland, *An Introduction to Random Vibrations and Spectral Analysis*, Longman, London, 1980.
18. A. C. M. Van Ette and H. J. Schoemaker, 'Harmonic analyses of tides—essential features and disturbing influences', *Proc. Symp. on Tides*, Monaco, 28–29 April 1967.
19. D. E. Cartwright and D. B. Catton, 'On the fourier analysis of tidal observations', *Int. Hydro. Rev.*, **40**(1), 113–125 (1963).
20. M. Miyazaki, 'A method for the harmonic analysis of tides', *Oceanogr. Mag.*, **10**(1), 65–80 (1958).
21. G. Godin, 'The resolution of tidal constituents', *Int. Hydro. Rev.*, **47**(2), 133–144 (1970).
22. H. Lamb, *Hydrodynamics*, Dover Publications, New York, 1932.